Long-term evolution and early warning strategies for complex rockslides by real-time monitoring

Crosta, G.B.[1], Agliardi, F.[1], Rivolta, C.[2], Alberti, S. [1], Dei Cas, L. [3]

(1) Department of Earth and Environmental Sciences, University of Milano-Bicocca, Piazza delle Scienza, 4, Milano, Italy, I-20126

(2) Ellegi s.r.l., Corso Magenta, 12, Milano, Italy, I-20123

(3) ARPA Lombardia, Settore Suolo, Risorse Idriche e Meteoclimatologia, Viale Francesco Restelli, 3/1, Milano, Italy, I-20124

Corresponding author:

Giovanni B. Crosta
Department of Earth and Environmental Sciences
University of Milano-Bicocca
Piazza della Scienza 4, Milano, Italy, I-20126; Building U4, room 2016.
Phone: +39-02-64482029; Fax: +39-02-64482073
E-mail: giovannibattista.crosta@unimib.it

Abstract

The potential of long-term, real-time surface displacement monitoring by ground-based radar interferometry (GB-InSAR) to improve the understanding of mechanisms and set up objective Early Warning criteria for complex rockslides is explored. Monitoring data for a rockslide in the Central Italian Alps, collected since 1997 by ground-based and remote sensing techniques, are examined. A unique 9-year continuous GB-InSAR monitoring activity supported an objective subdivision of the rockslide into "Early Warning domains" with homogeneous involved material, mechanisms and sensitivity to rainfall inputs. Distributed GB-InSAR data allowed setting up a "virtual monitoring network" by *a posteriori* selection of critical locations representative of Early Warning domains, for which we analysed relationships among rainfall descriptors and displacement rates. The potential of different Early Warning criteria, depending on the instability mechanisms dominating different domains, is tested. Results show that: a) rainfall Intensity-Duration-Displacement Rate relationships can be useful tools to predict displacements of "rainfall-sensitive" rockslide sectors, where clear trigger-response signals occur, but are unsuitable in rockslide domains affected by the long-term progressive failure of the rock slope; b) effective Early Warning strategies for collapse scenarios (entire rockslide, specific domains) can be enforced by modelling real-time, high-frequency GB-InSAR data according to the accelerated creep theory.

Keywords Rockslide, Monitoring, GB-InSAR, time to failure, warning thresholds, EWS, displacement, rainfall

1. Introduction

Large rockslides can evolve into rock avalanches, affecting landscape evolution and posing extraordinary risks. Their evolution depends on predisposing geological factors (e.g. rock type, structure, hydrology, seismic activity) and climatic factors (e.g. rainfall, snowmelt). Therefore, their activity often varies in time, with acceleration and deceleration periods depending on external factors and their relative combination in time, intensity and order of occurrence. Snowmelt and heavy rainfall are the main triggers of most annually recorded rockslide displacement in alpine environments (Cappa et al., 2004; Geertsema et al., 2006, Nishii and Matsuoka, 2010; Broccolato et al., 2011; Crosta and Agliardi, 2002; Crosta et al., 2012; Crosta et al., 2014).

Non-linear displacement trends and the superposition of seasonal or episodic effects make the prediction of the behaviour and time of failure of large rockslides a difficult task. Moreover, failure prediction is more difficult for large natural slopes than for engineered ones. In the latter case, a controlled excavation generally affects slope equilibrium rapidly by sharp changes in geometry and loading conditions, rapidly leading to progressive rock failure processes (i.e. induced by damage evolution of initial defects and controlled by the internal structures, heterogeneities, development of cracks at the micro- and meso-scale) quite well represented by "accelerating creep" theories and empirical models (Saito and Uezawa, 1961; Fukuzono, 1985; Voight, 1988; Rose and Hungr, 2007). Instead, natural rockslides evolve over longer times (up to thousands of years) under changing or cycling forces and triggers (e.g. glacial erosion and deglaciation, fluvial erosion, rainfall and snowmelt, seismic shaking), which act on slopes with evolving geometry and strength. Thus, rockslides often exhibit a combination of long-term creep-like deformation, related to progressive failure, and superimposed episodic or seasonal accelerations, related to hydro-mechanically coupled responses to rainfall or snowmelt (Cappa et al. 2004; Guglielmi et al., 2005; Zangerl et al., 2010; Crosta et al. 2014; Vallet et al., 2015). This can eventually result in continuous acceleration and catastrophic collapse (Voight, 1988; Fukuzono, 1985; Crosta and Agliardi, 2003; Sornette et al., 2004) or self-stabilization (Broadbent and Zavodni, 1982).

Accelerating slip trends detected over different timescales can provide some precursory signals for preparatory civil protection and emergency activities ("early warning"; Crosta and Agliardi, 2003; Bazin et al., 2012; Intrieri et al., 2012; Michoud et al., 2013). Nevertheless, occasionally the absence of displacement acceleration has lead to a false sense of security. Nevertheless, the quantitative analysis of such signals requires a continuous monitoring effort to be undertaken well before the onset of critical stages possibly preceding catastrophic collapse, and carried out for long enough to allow sampling of multiple successive "reactivation events" under repeated or exceptional triggering conditions. In the past, traditional monitoring activities have exploited point-like, local measurement techniques (topographic and ground-based geotechnical; Bhandari, 1988), usually in short-duration, low-frequency measurement campaigns. Although very useful to understand general landslide behaviour, these offered limited capabilities of: a) representing long-term landslide behaviour; b) attaining a spatially-distributed description of rockslide kinematics; c) understanding landslide sensitivity to perturbations and related response time, and event duration; d) collecting information for network implementation/maintenance; and e) providing suitable input to early warning. Recent advances in remote sensing have provided largely unexplored opportunities to overcome these limitations. Robotic total stations, continuous GPS and satellite (Ferretti et al., 2001, 2011; Strozzi et al., 2010) or ground based synthetic aperture radar interferometry (Tarchi et al., 2003) allow a more continuous and spatially distributed monitoring and mapping of surface displacement and velocity fields, while multiple LiDAR surveys can provide a detailed geometrical description. At the same time, automatic borehole durable probes can provide long-term continuous, high-frequency datasets to investigate landslide movements at depth (Crosta et al., 2014; Blikra et al., 2015).

The time-dependent behaviour of rockslide displacements can be reproduced by visco-plastic models (Angeli et al., 1996; Gottardi and Butterfield, 2001; Herrera et al., 2009; Ranalli et al., 2010; Puzrin and Schmidt, 2012; Secondi et al., 2012; Crosta et al., 2012, 2014) or impulse-response models based on statistical analysis and transfer functions (Bernardie et al., 2015; Vallet et al., 2015). Nevertheless, forecasting the final collapse phase remains difficult. The temporal pattern of displacements (slow vs. catastrophic, continuous vs. episodic) depends on the considered time window, stress boundary conditions, magnitude and temporal distribution of external actions, rockslide sensitivity to hydrological triggers (Broadbent and Zavodni, 1982; Crosta and Agliardi, 2003; Sornette et al., 2004; Faillettaz et al., 2010; Crosta et al., 2014). Starting from the direct observation that accelerating displacements preceding collapse exhibit a finite time singularity of the velocity, several empirical and physics-based models were proposed to predict the time of failure and the expected displacements of rockslides. Some rely on creep laws (Saito and Uezawa, 1961; Fukuzono, 1985; Voight, 1988; Rose and Hungr, 2007; Mufundirwa et al., 2010; Amitrano and Helmstetter, 2006) or phenomenological state- and velocity-dependent friction laws (Sornette et al., 2004; Helmstetter et al., 2004) to estimate the time to failure. These methods perform quite well in simple cases with continuous acceleration, but fail to provide reliable failure time estimates for rockslides with complex response to external actions, complex failure mechanisms, and material rheology changing with deformation and damage. In these cases, suitable monitoring activities are required to constrain rockslide kinematics and the temporal and spatial evolution of rock mass and shear zone properties (Crosta et al., 2014), and to establish correlations with triggers and predict future displacements or possible collapse.

Here we demonstrate the potential of long-term, spatially-distributed monitoring datasets provided by ground-based radar interferometry (GB-InSAR) to: i) explore the complexity of failure processes in large rockslides and identify domains characterized by different evolution to failure; ii) support the evaluation and selection of different approaches to Early Warning; iii) help minimizing uncertainties and false alarms in Early Warning activities. We exploit the Ruinon rockslide case study (Central Italian Alps) to develop a novel approach to the quantitative analysis of GB-InSAR data for process modelling and Early Warning. The approach consists of setting up “virtual monitoring networks” for landslide prediction and operational Early Warning purposes, based on refined geological models constrained by *a posteriori* evaluation of GB-InSAR displacement fields, collected over a representative observation period. We propose different approaches to establish displacement rate and rainfall thresholds for Early Warning, and discuss their advantages, limitations and the suitability of different descriptors to predict landslide evolution to failure.

2. The Ruinon rockslide

The Ruinon rockslide affects the right hand flank of the Valfurva in the Upper Valtellina (Central Italian Alps; Fig. 1a), characterized by a continental-alpine rainfall regime (i.e. rainy summer and autumn) with annual average, maximum, and minimum rainfall of 750, 1300, and 300 mm, respectively. Slope instability involves pre-Permian phyllites of the Austroalpine Campo Nappe, as well as glacial and talus deposits (Crosta, 1999, 2000; Agliardi et al., 2001). The rockslide is nested into a larger deep-seated gravitational slope deformation (DSGSD), which affects the entire slope from 1450 m a.s.l. up to 3000 m a.s.l. (Fig. 1b). The Ruinon rockslide is characterised by two major scarps, namely: the Upper Scarp (US, 2100 m a.s.l.), exposing disturbed rock masses, and the Lower Scarp (LS, 1950 m a.s.l.), involving disintegrated rock mass and a thick debris cover (Fig. 1c). The occurrence of ESE trending trenches upslope of the US and of a large Holocene rockslide accumulation close to the active rockslide (Figs. 1 and 2) suggest: a) structural links between the Ruinon rockslide and the larger DSGSD; b) a long-term evolution of the rock slope instability; c) a retrogressive evolution of the Ruinon rockslide up to 2200 m a.s.l., in a slope sector with highly fractured bedrock. Minor, shallow slope instabilities associated with the rockslide are widespread, including fragmental rockfalls (mainly at the US and right rockslide flank) and debris slides/debris flows (LS and downslope areas).

Although first evidence dates back to early 20th century, the rockslide became more active since 1960 and underwent accelerations in 1983, 1987, entering a significant progressive stage between 1997 and 2003. This is suggested by the evidence mapped on the available aerial photo series.

The rapid evolution of the rockslide motivated the deployment of site investigations, carried out in stages between 1988 and 2013 (Fig. 2) and including 14 boreholes (up to 190 m long) instrumented with inclinometers and standpipe piezometers. 10 boreholes provided fully-logged drill cores. Borehole data supported the interpretation of the geometry, kinematics and hydrology of the rockslide (the latter still not fully resolved). The Ruinon is a compound rockslide affecting about 15 Mm^3 (Fig. 3) with shear zones localized at 30 to 70 m in depth (Crosta, 2000; Agliardi et al., 2001; Crosta and Agliardi, 2003; Casagli et al., 2010). The potential daylighting zone of the rockslide failure surface (1700 m a.s.l., outlined by groundwater spring lines slightly changing position with time) is hanging above the valley floor (1450 m a.s.l.), possibly leading to evolution into a rock avalanche in case of catastrophic failure (Fig. 2). Evidence of upslope expansion (Fig. 2 and 3) suggests a total unstable volume potentially reaching up to 20 Mm^3.

3. Rockslide monitoring system

Rockslide displacement measurements have been carried out since 1997 by a ground-based network (up to 25 wire extensometers and backup distometer baselines, 17 GPS, optical targets, 2 borehole inclinometers, 1 borehole multibase extensometer), and in recent years by radar interferometry (i.e. satellite-based PS-InSAR™ and SqueeSAR™, and ground-based GB-InSAR™). The monitoring network covers the rockslide area and is denser around the US and the LS (Fig. 2). While inclinometer tubes were rapidly damaged allowing only few measurements, the monitoring network provided the longer and more continuous time series of surface displacements for a rockslide (>18 years).

3.1. Ground-based network

Data provided by the ground-based monitoring network (Fig. 4) allowed identifying rockslide sectors with different styles of activity and response to external triggers. Crosta and Agliardi (2003) identified three different patterns of displacement, namely: "brittle", with stick-slip movement of limited rock volumes; "chaotic", observed in areas of debris/disrupted rock and lacking a well-defined temporal trend; and "seasonal creep" (Fig. 4), with non-linear acceleration phases during wet seasons and resting periods during winter and early spring. Seasonal "reactivations", associated to rainfall and snowmelt, were superimposed over a generally progressive (i.e. accelerating) trend from 1997 to 2002 (Fig. 4), whereas a stage of long-term stabilisation took place between 2003 and 2007. From 2008, the rockslide started accelerating again over the long-term, suggesting that "progressive" behaviour occur at different timescales due to a complex interaction between rock failure mechanisms and the superposition of precipitation and groundwater recharge events.

3.2. Satellite-based radar interferometry

Satellite InSAR data processed by the Permanent Scatterers^{TM} and the SqueeSAR^{TM} techniques (Ferretti et al., 2001, 2011) are available for the study site. They cover a time span of about 17 years by exploiting different imagery (ERS1-2 1991-1999, Radarsat S3, 2003-2008), and provide spatially-distributed displacement data spread over the entire slope, including sectors upslope and outside the rockslide area. Measured SqueeSAR^{TM} displacement rates (Fig. 5a) prove the activity of the DSGSD, with average values between 15 and 25 mm/yr and maxima of 35 mm/yr along the satellite Line-of-sight (LOS). Displacement rates decrease moving to the toe, theoretically supporting a non-planar DSGSD sliding mechanism.

3.3. Ground-based radar interferometry

In order to monitor the rockslide displacement field, a LiSALabTM GB-InSAR system was installed in June 2006 (Casagli et al., 2010) and has been providing continuous operation for more than 10 years. The active sensor is located on the opposite valley slope at 1775 m a.s.l. (Fig. 3), at a distance from the rockslide ranging between 1000 m (rockslide toe) and 1800 m (US) along the line-of-sight. The system, initially installed as part of a research experiment (Tarchi et al., 2003; Antonello et al., 2004; Casagli et al., 2010), was incorporated in the near real-time monitoring network operated for civil protection purposes. In the present configuration, the LiSALab system uses a microwave transceiver unit working at Ku band (12-18 GHz) with a licensed central frequency of 17.35 GHz (bandwidth of 100 MHz) and generating a synthetic aperture antenna of about 3 m and illuminating about 50% of the rockslide area and upslope sectors up to a maximum distance of about 4 km, embracing the Cima di Saline ridge (Fig. 5b).

A 1-year (2006-2007), long-range GB-InSAR experiment (Fig. 5b), provided displacement time series (with values exceeding 20 mm/yr) which were compared to satellite InSAR data (Fig. 5a) both for slope debris (sector 1 in Fig. 5b) and rocky outcrops within the DSGSD (sector 2 in Fig. 5b).

The permanent monitoring settings of the system allow acquiring radar images and displacement maps with a theoretical range resolution of 1.5 m and a theoretical azimuthal resolution between 2.6 and 5.2 m.

The scanning time for each image acquisition and the statistical averaging interval considered to improve the quality of the radar images, vary from minutes to hours. During periods of normal landslide activity, the scanning time and the statistical time window are about 14 minutes (approximately 4-5 images per hour) and 6-hours, respectively. These time intervals can be decreased down to two minutes during critical acceleration stages to resolve the possible phase ambiguity and avoid phase wrapping.

The accuracy of the system set up under optimal measuring conditions (high scene coherence with high SNR, negligible atmospheric effects, lack of vegetation; Tarchi et al., 2003) amount to a very small fraction of the signal wave length (λ) and can reach sub-millimetric values. Of course, limitations to the accuracy and completeness of radar data can derive locally (in space and time) from increased noise due to vegetation, un-resolvable atmospheric effects and Line-of-sight obstructions.
The system has been equipped with rugged high-speed data transmission connections, redundant power supply, near real-time connection with a weather station, and time-lapse webcams. The system now provides the most comprehensive and integrated information about the rockslide behaviour, in order to support the risk mitigation actions requested by the civil protection plan. In this perspective, the LiSALab system provides near- and real-time results in terms of: a) geo-referenced pseudo-3D maps of Line-of-sight (LOS) displacements, obtained by converting local radar coordinates to global coordinates (X,Y,Z) using a reference Digital Elevation Model; and b) streaming time series of displacement at selected points of interest (POI). Since displacements are resolved only along the radar LOS, the recorded component of the local displacement vector slightly varies at each slope location. This usually implies an underestimation of real displacements, which is minimized by optimizing system positioning and quantified by ground-truthing. In this case, data from ground-based instrumentation (Fig. 2) allowed validating the spatially-distributed displacement data provided by the GB-InSAR system since 22 July 2006. The comparison between GB-InSAR and wire extensometer data (Figure 6) at corresponding locations proved the consistency of radar measurements, with extensometer data often providing upper bounds. GB-InSAR data were also validated through local measurements by total station and optical targets where they were available.

4. Advanced analysis of GB-InSAR displacement data

4.1. Data processing for rockslide model refinement

The spatially-distributed nature of GB-InSAR measurements supported a refinement of the rockslide conceptual model and the analysis of rockslide mechanisms and sensitivity to triggers for Early Warning purposes. In a first stage, we systematically analysed displacement data from June 2006 to February 2010 (Fig. 7), and automatically extracted GB-InSAR displacement maps as 5483 geo-referenced GridAscii files (one every 6 hours; grid size: 1500x1500 pixels; cell size: 1 m) for further raster processing in a GIS environment. For each pixel we cumulated measured displacements over 30-day periods to obtain multi-temporal Cumulative Displacement maps (CDM), and monthly Incremental Displacement maps (IDM) (Fig. 7). Preliminary analysis of monthly CDM allowed resolving the rockslide displacement fields and a first identification of sub-areas characterized by cumulative displacement magnitudes and patterns consistently different over the considered time period. This was based on the assumption that the latter may reflect different landslide mechanisms (e.g. shallow to deep-seated) and different sensitivity to hydrological forcing (Fig.7 a-c). On the other hand, IDM provided unique insights in the temporal pattern of the displacements, and allowed highlighting both seasonal behaviour and episodic acceleration events, mapping rockslide sectors evolving in specific time periods (Fig. 7 d-f), and discovering nested landslide sub-sectors. The latter are characterised by independent kinematics in debris areas where traditional ground-based instrumentation would be impossible to install or easily damaged or difficult to maintain (e.g. debris slide near rockslide toe, Fig. 7d).

4.2. Definition of rockslide sub-areas: Early Warning domains

The subdivision into sub-areas was refined through geomorphological mapping (Fig. 8a) based on multi temporal aerial photo-interpretation (on photos taken in 1954, 1976, 1982, 1997, 2000, 2003, 2007, 2010, 2013) and field mapping, aimed at identifying the extent of debris-covered areas and their changes, areas of outcropping rock, major structures, and kinematic evidences.

This analysis identified 13 rockslide sub-areas, each one characterized by an homogeneous set of geomorphological features, behaviour and style of activity, depending on the affected material (e.g. bedrock, fine or coarse debris) or on local structural controls. Sub-areas have been grouped into 7 larger "Early Warning domains" (A to G, Fig. 8b) representative of different failure scenarios in a practical Early Warning perspective.

EW domain "A" includes a fast moving area (>10 m since 2006) characterised by the mixed sliding and toppling of extremely fractured rock masses at the eastern tip of the Upper Scarp (US). EW domain "B" includes the US crown, characterised by smaller displacements (typically 4-5 m since 2006) and providing a passive feedback of the global rockslide movement. It represents the boundary between the faster part of the rockslide (downslope) and the slower upslope sector affected by retrogressive activity. A fast reactivation of such domain would provide an important evidence of transition to catastrophic collapse of the entire rockslide. EW domain "C" (displacements up to 10 m since 2006) includes the rockslide head sector, mantled by a thin debris cover, and provides a figure of the deep-seated rockslide movement. A similar interpretation applies to domain "D", which includes the steep sector of the Lower Scarp (LS) formed by both coarse debris and outcropping bedrock. EW domain "E" consists of the thick debris covering pre-existing reworked glacial deposits, with masked bedrock outcrops downslope of the LS. This sector, locally affected by groundwater spring occurrence and displacements up to 50 m, showed a high sensitivity to rainfall and snowmelt by releasing debris flows and debris slides. EW domain "F" is close to domain "E", but consists in a large independent debris slide undergoing acceleration stages, which could also destabilize domain "E". Finally, EW domain "G" includes two slope sectors located at the right and left hand rockslide sides and so-far characterized by negligible movements. Because of their peripheral position, stability through the 17 years of monitoring activities, and prevalent good quality rock mass, they may provide passive feedbacks for global catastrophic failure or rockslide enlargement.

4.3. Extraction of displacement time series: virtual monitoring network

Displacement monitoring data provided by traditional, point-like geotechnical instrumentation are susceptible to local biases or incorrect placement. The spatially-distributed nature of GB-InSAR data provides the opportunity to set up extensive monitoring networks by *a posteriori* selection of monitoring locations representative of the evolution of different rockslide EW domains. We adopt this innovative approach to set up a network made of "virtual sensors" distributed along representative profiles, aligned or transversal to the EW domains (Fig. 8b). Based on radar Cumulative Displacement Maps, we selected 205 monitoring points (each corresponding to a GB-InSAR slope cell. For each cell, we extracted a displacement time series by sampling the entire stack of Cumulative Displacement maps (one every 6 hours) over the period June 2006 to November 2014. Within the obtained dataset, we selected 132 cells providing continuous time histories over the entire monitoring period (Fig. 9). Data have been further processed to remove the effects of "phase wrapping" during critical periods of increased activity. Corrected time series allowed a further quantitative check of rockslide sub-area zoning and the selection of a set of 21 virtual sensors for operational early warning purposes (Fig. 2). We considered time series extracted at these points to evaluate the sensitivity to external triggers and deploy suitable early warning criteria for EW domains. We also performed specific analyses of the critical reactivation periods observed on October-November 2012, 2013 and 2014.

5. Objective definition of Early Warning criteria

The design of a landslide Early Warning system (EWS) includes: a) definition of system behaviour, mechanisms and sensitivity to triggering actions; b) identification of relevant changes in the system status (e.g. acceleration, failure) and associated probabilities and risk scenarios; c) definition of criteria (thresholds) to detect critical changes in sufficient advance to allow undertaking suitable actions; d) implementation of operational procedures to manage critical changes and the return to ordinary conditions; e) definition of requirements for updating threshold values following changes in system behaviour (Crosta and Agliardi, 2003; Crosta, 2013).

Establishing quantitative early warning thresholds for large rockslides is difficult, due to their complex kinematics, interaction between long-term progressive failure and hydro-mechanical coupling, and changing mechanical and hydraulic properties (Crosta et al., 2014). Long-term and seasonal behaviours usually make difficult to discriminate between long-term creep and hydrologically-driven deformation components, and even to clearly identify trigger-response relationships (Bernardie et al., 2015). In fact, large rockslides can respond in different ways to similar triggering actions depending on the season, the cumulative effect of different inputs and the relative contribution of ongoing progressive rock failure processes. We propose a new methodological approach to the evaluation and implementation of different possible Early Warning approaches on the basis of radar displacement time series.

5.1. Landslide sensitivity to hydrological triggers: selecting Early Warning strategies

Defining suitable Early Warning criteria for complex rockslides requires assessing relative contributions of long-term creep (e.g. progressive failure) and hydrologically-driven failure processes to the measured displacements. This is key to understand which aspect of landslide behaviour (i.e. reactivation/acceleration, triggering of shallow or deep-seated debris slides / debris flows, global rockslide collapse) can be predicted by monitoring a specific slope sector.

The response of the Ruinon rockslide to external inputs varies in intensity and delay. With some exceptions for the snowmelt season (April to June), displacements are recorded during rainy periods (late summer-early fall), with cumulative displacements following cumulative rainfall trends on long, annual and short-term (Figs. 9, 10 and 11). In the dry and cold seasons, the rockslide slowly creeps in most of the sectors, with the slower movements recorded in the rocky sectors at rockslide boundaries ("B" and "G"; Figs. 9 and 10). Snowmelt can explain local displacements in absence of rainfall, whereas the coupling of occasional early snow fall with intense rainfall events can result in extreme accelerations and cumulative displacements (e.g. October 2012, 2013, 2014). A qualitative evaluation of cumulative rainfall and cumulative displacement plots (Fig. 9, 10 and 11) suggests that the rockslide sensitivity to rainfall depends on the considered rockslide sector and on the type of rainfall input (i.e. long-term cumulative input, rainy period, close sequence of storms). EW domains "A" and "E" (i.e. sectors with thick debris cover) are characterised by large displacements (up to 2m/yr) following well-defined short periods of intense rainfall or snowmelt. The EW domain "F" (i.e. debris slide downslope of LS) also undergoes large displacements with maximum response associated to longer duration rainfall. On the opposite, EW domains "B" and "G", embracing the rocky US and rockslide flank, appear less sensitive to rainfall inputs, with total displacements in the monitoring period being less that one tenth of those observed downslope of LS. Along the US (domain "B") displacement shows a long-term creep trend, whereas most of the superimposed annual displacements occur until early spring, suggesting that the role of snowmelt is more relevant than rainfall inputs in controlling the deep seated slide movement. In these sectors, displacements seem to closely follow global rockslide failure scenarios. EW domains "C" and "D", also mirroring deep-seated rockslide movement, follow quite closely the seasonal-scale rainfall patterns, but show more complex responses to individual rainfall periods.

We quantitatively assessed the relationship between rainfall and rockslide activity by the analysis of antecedent rainfall. Most published analyses refer to shallow soil slope instabilities and earth slide/flow landslide types (Crosta et al., 2010), whereas very little is available for deep rockslides. Time series of antecedent rainfall, cumulated over 1, 7, 15, 30, 45, 60, and 90 days, were derived from available datasets and compared to corresponding distributions of displacement rates, measured at each radar streaming point during a "training" period (June 2006-June 2011). Boxplots (e.g. Fig. 12) representing the distributions of displacement rates for different classes of cumulative antecedent rainfall were prepared for all the streaming points of each EW domain. We selected mean values of displacement rate from boxplots to generate curves of displacement rate versus rainfall, cumulated over different reference periods. The curves obtained in this way for each streaming point (3 curves for EW domains "A", "B", "C and "D"; 5 curves for domain "E"; 2 curves for domains "F" and "G") have been averaged considering points within the same rockslide sector. These final curves should represent the average response to rainfall of each rockslide EW domain (Fig. 13). In general, we observe a slight increase of displacement rates with the rainfall accumulated in a reference period, until a threshold value, which is different for each EW domain. From then on, a sharp increase in displacement rate is observed with different trends, suggesting that the rockslide response magnitude depends on the rockslide sector and on the rainfall amount cumulating period (Figs. 12 and 13).

In particular, EW domain "A", involving the continuing failure of coarse disrupted rock material shows the highest sensitivity to rainfall inputs with sudden and significant short-term responses even to small rainfall inputs (Fig. 14). EW "E" and "F", involving thick debris material at and below the LS show significant response to 7 to 15-day cumulative rainfall inputs, suggesting that a certain amount of groundwater recharge is required to trigger acceleration of relatively deep failures affecting thick debris cover. Rockslide domains made of bedrock covered by a thin mantling debris ("C" and "D") or by outcropping rocks ("B" and "G") show a low sensitivity to rainfall inputs, which decreases with increased cumulating periods (Figs. 13 and 14). For rainfall-sensitive domains, 7 and 15 day are the time intervals for which a non-linear relationship between cumulative rainfall input and displacement rate is more evident. The threshold value of cumulative rainfall beyond which displacement rate increases rapidly ranges between 50 and 100 mm. For longer time periods (i.e. 30-60 days), rainfall threshold values rise to about 200 mm (Fig. 14).

5.2. *Predicting landslide displacements: Intensity-Duration-Displacement Rate relationships*

We quantitatively analysed individual rockslide sector response to specific weather events by isolating displacement rate curves for specific precipitation events (Fig. 15). We defined as "individual rainfall events" those following a "dry period", and characterized by a 24-hour antecedent rain and a 15 day cumulative rainfall lower than 5 mm and 20 mm, respectively. In order to ensure a complete exhaustion of the displacement curve before the start of a subsequent event, we also considered that no rainfall must occur in the 5 days following the rainfall event. These constraints help obtaining a dataset of rockslide responses to individual rainfall events minimizing the superimposition of effects associated to multiple rainfall events or short term antecedent conditions.

We identified 70 rainfall events which satisfy the imposed conditions, with variable duration (5 hours to 13 days), cumulative rainfall height (50 to 312 mm), and season of occurrence (April to October). Rainfall time series available at hourly resolution have been compared to rockslide displacement rates averaged over 4 measurements to filter displacement data from noise. We focused on the rockslide behaviour over the period of "reactivation" which starts with the rainfall event and ends up when displacement rates return to their reference long-term pre-rainfall value. This usually occurs within 1-5 days after the conclusion of the rainfall event (Fig. 15).

Typical responses of all the radar streaming points in rainfall-sensitive EW domains (e.g. “A” and “E”; Fig. 15) are characterized by a peak-exhaustion behaviour, with displacement rates (averaged over 6-hour intervals) increasing to a maximum (0.3–5 mm/6hr) and then slowly decaying to “long-term” value (e.g. 0.04 mm/h for domain “E”). Response of different monitoring points belonging to the same domain is almost completely synchronous but of different magnitude (i.e. peak value). Peak displacement rates measured for each rainfall event are generally within 10-20 mm/day with maxima reaching 24 mm/day. The time lag between displacement rate peak and main rainfall input amounts generally to 1–2 days. The decreasing limb of the displacement rate vs. time curves is less steep than the rising one, and the perturbation usually exhausts within 3-5 days, with some cases up to 10 days depending on the duration and total amount of precipitation.

On the other hand, EW domains “B” and “G” do not show clear single peaked responses to short-term precipitation inputs, but small “stick-slip” (EW domain B) multi-peaked or noisy displacement rates (EW domain G) can be observed (Fig. 15). These results suggest that rainfall-response plots can be used as screening tools to test the suitability of rainfall thresholds as potential Early Warning tools depending on the observed behaviour of rockslides or rockslide sub-areas.

For EW domains clearly sensitive to rainfall inputs, we attempted a definition of rainfall-displacement rate relationships by assuming that: a) rockslide response to each forcing event is a function of its intensity and duration, the specific sensitivity of the considered landslide domain, the involved mechanism and seasonality; b) trigger-response relationships are reasonably stable in time; c) 8 years of monitoring data include a spectrum of rainfall events allowing for a representative analysis.

We apply this approach, similar to that of Del Ventisette et al. (2012), to unravel the behaviour of the rockslide to weather forcing and verify its suitability as an Early Warning tool. In our “individual rainfall event” dataset, we selected 27 rainfall events with different characteristics and covering the period between April and November (2 in April; 3 in May; 4 in June; 4 in July; 2 in August; 5 in September; 6 in October; 1 in November). For each event, we evaluated cumulative displacement, mean and maximum displacement rate, time-lag from rainfall onset and total duration. The intensity of rockslide response to each rainfall event varies locally depending on the rainfall patterns. Mean displacement rate has been computed as the ratio of the cumulative displacement over the event duration and maximum displacement rate from the ratio of the cumulative displacement, from the event onset to the peak velocity, and the time to peak.

For each radar streaming point of each EW domain, this analysis allowed plotting intensity-duration (I-D) data, classified by the associated measured displacement rates, thus obtaining “Intensity-Duration-Displacement Rate” (IDDR) plots. Fig. 16 shows the different trend and distribution between monitoring points representative of “rainfall-sensitive” (debris or disrupted rock masses) or “rainfall-insensitive” (rock mass) domains. In “rainfall-sensitive” domains, I-D values characterised by similar displacement rate show clear linear trends in a log-log plot, which shift upward for increasing displacement rates (Fig. 16). For “rainfall-insensitive” points, the same progressive upward shifting cannot be observed. In this case, possible signals are masked by noise, thus demonstrating the unsuitability of this approach for Early Warning in domains lacking clear rainfall-displacement responses (Figs. 15 and 16).

5.3. Predicting landslide collapse: Early Warning velocity thresholds

Modelling the failure mechanisms of complex rockslides requires a detailed knowledge of rockslide geometry and structure, the constitutive behaviour of the involved materials, from initial failure to rapid collapse, as well as the boundary conditions and related variations in space and time (e.g. internal fracturing, shear zone development and relative changes in properties, Crosta et al., 2014). This is usually unfeasible for real-time Early Warning applications, because of the large dataset required, the time required by model running and calibration tasks, and the uncertainties underlying modelling assumptions and the modelling. Several empirical/phenomenological approaches exploiting the analysis of time series of monitoring data, based on the “accelerating slope creep” theory (Saito and Uezawa, 1961; Fukuzono, 1985; Voight, 1988; Rose and Hungr, 2007) were proposed to overcome some of the above-mentioned difficulties. For large landslides with complex kinematics, displacement trends and response to external triggers, Crosta and Agliardi (2003) proposed a methodology to obtain physically-based alert velocity thresholds. The method, based on the Fukuzono-Voight equation (Voight, 1988), establishes a non-linear relationship between acceleration and displacement rate. The proposed equation provides a description of accelerating (i.e. tertiary) creep:

$$\Omega = \frac{1}{A(\alpha-2)}\left\{\left[A(\alpha-1)t_f + \dot{\Omega}_f^{\,1-\alpha}\right]^{(2-\alpha)/(1-\alpha)} - \left[A(\alpha-1)(t_f - t) + \dot{\Omega}_f^{\,1-\alpha}\right]^{(2-\alpha)/(1-\alpha)}\right\} \qquad \text{(Eq. 1)}$$

with: $\alpha>1$, $\alpha\neq2$, $A>0$ and $t_f>t$, t_f is the failure time associated to the assumed failure rate (i.e. infinite or having a specific high value), α and A are dimensionless constants controlling the sensitivity of accelerating activity and the curve shape (Crosta and Agliardi, 2003). The equation applies under the assumptions of: a) continuous acceleration; b) constant stress. These conditions are not satisfied in unstable real slopes, but are more easily met for fast evolving single collapses in mining environments, where the inverse velocity approach has been succefully used (Fukuzono, 1985; Rose and Hungr, 2007). Large landslides are frequently characterized by significant changes in geometry and loading conditions (i.e. non-constant stress), changing rheology (i.e. A and a are not constants) and hydrologically-controlled seasonal displacement patterns superimposed on long-term slope creep (i.e. landslide is not continuously accelerating). These issues usually hamper a realistic or reliable estimation of the time to failure of complex rockslides.

Crosta and Agliardi (2003) used the Voight’s equation, integrated to a power law of displacements versus time (eq. 1), to fit the Ruinon time series of measured cumulative displacements (Fig. 17a) and derive model parameters (namely, A, α, and t_f). Also Sornette et al. (2004), after observing that some of the parameters in their slider-block friction model were poorly constrained by the inversion process, proposed to fit cumulative displacement data. From the estimated parameters, synthetic velocity-time curves can be derived (Fig. 17b), providing a quantitative basis to establish alert velocity threshold values. These correspond to different time intervals before expected failure (irrespective of the real, unpredictable time of failure) and can be useful for Early Warning. Seasonality can be described analytically adding a periodic component (Fig. 17c) to Eq. 1. This shows that the superimposed periodic acceleration/deceleration is relevant far from the final collapse. Getting closer to the final acceleration phase the step-like trend disappears with shorter plateau portions as the curve evolves progressively into the asymptotic trend. This decoupling could become more evident for changes in material properties occurring at increasing displacement or velocity.

The method of Crosta and Agliardi (2003) was originally based on data from ground-based instrumentation (e.g. distometer baselines, wire extensometers, total station measurements). Nevertheless, GB-InSAR monitoring approach appears even more suitable to apply this forecasting approach to both debris and deep seated rock instabilities by providing: a) high coverage spatially-distributed data; b) real-time measurements; c) high-frequency measurements providing nearly instantaneous velocity estimates; d) acquisition also in difficult environmental conditions. For the Ruinon rockslide, we fitted time series of cumulative displacement corresponding either to the entire monitoring period or specific critical accelerating periods (e.g. April-July 2008 and October-November 2012) at the 21 representative “virtual sensors” spread over the 7 EW domains (Fig. 8), using eq. (1). Early Warning is enforced by the regional authority at each virtual sensor by the real-time comparison between measured displacement rates (averaged over 6 hours) and three velocity thresholds (Figs. 14 and 15) corresponding to pre-alert, alert and emergency conditions. EW thresholds need to be updated as landslide geometry and rheology progressively change due to accumulation of deformation and damage, and to the seasonal effects which strongly modify the applied stresses and available strength. These changes in landslide behaviour (and corresponding critical conditions) have been partly accounted for by adapting the reference time intervals “before failure” to different combinations of intensity of triggering events and rockslide sensitivity (Fig. 18). Periods of 7, 15 and 30 days before failure were used until 2012 for the “emergency”, “alert” and “pre-alert” warning levels, respectively (see Crosta and Agliardi, 2003). After 2012, they became unsuitable to forecast shallow sliding scenarios in debris covered areas, especially following rapid snowmelt and rainfall. In these cases, reference time periods were reduced to 2, 3 and 4 days (Fig. 18).

5.3.1. Analysis of false alarms

An efficient Early Warning System (EWS) should in general minimize the rate of false alarms, which affect risk perception and pose problems to the technical and decision-making staff in charge of the monitoring network, the population, and local administrations affected by the emergency plan and actions. These usually involve costs relative to the alternative transportation of goods and people, the closure of main and sometimes unique roads, and consequently of industrial and commercial activities, the extra hours to be paid to the involved personnel for managing the emergency actions and the monitoring network, the loss in tourism revenues.

The problem of false alarm reduction can be tackled using different approaches: a) adopting higher threshold values; b) increasing redundancy: threshold values must be exceeded for more than one sensor within the same region of interest; c) introducing pre-alerting thresholds for a step-by-step verification of critical conditions; d) joint use of different indicators (e.g. displacement, velocity, acceleration, rainfall) for areas with different sensitivity to forcing factors, or areas subjected to different scenarios; e) threshold adaptation in case of local changes in behaviour with consequent change in the representativeness of monitored points.

The long term records of the Ruinon rockslide allowed to test different Early Warning threshold enforcement approaches on the recorded rate of false alarms. Velocity thresholds have been applied to verify the number of alerts and false alarms that could have been sent out during the 7 years long GB-InSAR monitoring period. Furthermore, the recent 2012, 2013 and 2014 events are useful to further validate the approach. Fig. 19 shows the number of false alarms by comparison of the recorded displacement rates with the threshold values implemented according to different approaches. Exceedance of the threshold value for a single streaming point in a specific EW domain causes a large number of false alarms (see Fig. 19a), whereas exceedance of the maximum threshold value within each EW domain (Fig. 19b) reduces the total number but locally can still generate frequent false alarms. Adoption of threshold values computed over a longer time interval (20 days) eliminates some of the alarms especially for areas in rocky masses, where noise can cause instantaneous exceedances. Updating the thresholds for the EW domain D after the 2012 event improves again the performance of the warning system, in terms of minimization of the false alarms.

6. Discussion and conclusions

Early Warning Systems for large, complex landslides require the definition of threshold values for specific indicators, commonly: displacement, displacement rate, rainfall (e.g. intensity, duration), pore water pressure or piezometric level. We propose a novel workflow to define quantitative EW thresholds for complex rockslides in steps, including: a) identification of different “EW domains” depending on their observed behaviour; b) analysis of individual EW domains to interpret associated monitoring data (e.g. local failure in debris vs. global rockslide failure) and select suitable variables to be used for early warning; c) definition of EW thresholds for hydrologically-driven landslide displacements, provided that site-specific trigger-response relationships apply; d) definition of EW thresholds for landslide collapse scenarios, by the accelerating creep theory; e) optimization of EW threshold values and implementation criteria to minimize false alarms.

Displacements are the most used descriptors of landslide activity and evolution. Displacement data at depth are generally more significant, could be associated to specific failure scenarios and to a precise triggering time by measurements of the pore pressure or piezometric level. On the other hand, deep displacement data are rarely continuous over long time in rockslides characterized by large deformation rates, and are usually point-wise or collected along lines (e.g. borehole inclinometers) and discrete in time. Surface displacements integrate the effects of deep failure mechanisms and internal deformation of the rockslide body, are generally affected by more complex patterns and are triggered before deep ones. Nevertheless, they can be easily measured over long time periods in a spatially-distributed way, thus providing unique datasets for EW domain identification and characterization.

To this aim, the integrated use of GB-InSAR and traditional, ground-based geotechnical monitoring has become an extremely powerful tool for understanding the behaviour of landslides and to design, set up and manage an Early Warning system. In the past, remote monitoring techniques and GB-InSAR data have been mainly used to map and follow slope instability, but rarely for a deeper understanding of landslide mechanisms or quantitative predictions of slope deformation and failure. Our novel approach to the quantitative analysis of GB-InSAR data consists in setting up *a posteriori* monitoring networks, characterized by an improved capability of mirror specific mechanisms or aspects of slope instability, by fully exploiting radar displacement fields. Data, validated by ground-based measurements, allows identifying homogeneous rockslide sub-areas and interpreting their behaviour in order to establish domain-specific warning thresholds consistent to the dominant deformation and failure processes mirrored by monitoring data in different domains.

Rainfall thresholds for rockslide “reactivation” can be based on an accurate analysis of landslide sensibility to different perturbations and both antecedent and event rainfall amounts can be used and related to observed/expected displacement rates. The analysis of relationships between individual rainfall events and the resulting landslide response allows screening the sensitivity of different domains to hydrological triggering, and thus the suitability of different alerting approaches (displacement rate thresholds or rainfall intensity and duration thresholds) to be used in the operational management of civil protection actions accordingly. On the other hand, EW thresholds aimed to predict the collapse of rockslides or sub-sectors require: a) knowledge of behaviour recorded for similar landslides; b) long term monitoring records; c) identification of the characteristics of the triggering events; d) revision of the landslide behaviour and consequently of the thresholds when landslide material undergoes major changes (in properties and behaviour). These points suggest the need for an adaptative (partially observational) approach to succeed in the management of an EWS.

Once suitable EW thresholds have been selected, a major issue for complex landslide settings is the choice of the critical reference points to be followed for monitoring activities and issuing of the warnings. For the described case study, EW domains “B” and “D” could be critical when used for managing the Early Warning System. Both sectors have a small vertical extent so that they could evolve quickly requiring an updating of the monitored points by choosing new representative point locations after each relevant reactivation event. This is even more evident for sector “D”, which is limited downslope by the more active and rapidly evolving sector, annually characterized by meter displacements.

In addition, as mentioned above large landslides undergo complex evolution over the long-term, depending on progressive material degradation, increase in rock mass fracturing and consequent change in hydraulic and mechanical properties, strain localization at depth and generation of shear zones subject to progressive comminution which can initially favour and subsequently occlude groundwater flow (Crosta et al., 2014). All this suggests that the rockslide sensitivity to triggering changes with time and the corresponding EW thresholds should consequently evolve in time, to avoid the occurrence of unforeseen behaviours or of frequent false alarms.

To tackle the false alarm problem, we proposed different methods including: a) careful averaging or filtering of the measurements. This will smooth the dataset avoiding the exceedance of threshold values because of instantaneous peaks, noise or local external disturbance; b) introduction of a condition of multiple simultaneous exceedance of EW thresholds for a specific indicator at different points (multiple sensors). This is fundamental for complex landslides, where different types of behaviour occur at different times or in different positions; c) as in b), but with contemporaneous exceedance of more than one indicator (e.g. displacement rate and piezometric level or rainfall); d) differentiation of landslide portions characterized by different behaviour and consequently with a different signal-to-noise ratio. This is important because it could imply the definition of different threshold values or an appropriate filtering and averaging approach. e) Regular update of threshold values and eventually the indicators to follow the evolution of the landslide, both in time and space, the change in material properties (physical and mechanical, both of the landslide mass and basal shear zone) or in boundary conditions (e.g. groundwater recharge, vegetation growth). A combination of these different approaches can lead to a flexible and reliable management of a EWS.

Acknowledgments

We thank ARPA Lombardia for collaboration, and Davide Leva (Ellegi s.r.l.) for continuous development of the LisaLab GBInSAR software and equipment and the help in data analysis. We are grateful Regione Lombardia for providing satellite-based radar interferometry data (TRE - Telerilevamento Europa srl). The research was partly supported by the EU FP7 project SAFELAND - (GA 226479), and partly by the Italian Ministry of Research – PRIN 2010-11 program prot. 2010E89BPY_007 project. Data presented and discussed in this paper can be requested directly to the authors.

References

Agliardi F., Crosta G., Zanchi A. (2001). Structural constraints on deep-seated slope deformation kinematics. Engineering Geology 59 (1-2), 83-102. doi:10.1016/S0013-7952(00)00066-1.

Amitrano D., Helmstetter A. (2006). Brittle creep, damage, and time to failure in rocks. Journal of Geophysical Research. 111: B11201.

Angeli M.G., Gasparetto P., Menotti R.M., Pasuto A., Silvano S. (1996). A visco-plastic model for slope analysis applied to a mudslide in Cortina d'Ampezzo, Italy. Quarterly Journal of Engineering Geology and Hydrogeology, 29(3), 233-240.

Antonello, G., Casagli, N., Farina, P., Leva, D., Nico, G., Sieber, A. J., Tarchi, D. (2004). Ground-based SAR interferometry for monitoring mass movements. Landslides 1(1), 21-28.

Bazin, S., Malet, J-P., Damiano, E., Picarelli, L., Cardellini, S., Garbarino, E., Gozzi, A., Lovisolo, M., Baron, I., Jochum, B., Ottiwitz, D., Supper, R., Kumelj, S., Bye, L.M., Eidsvig, U., Kalsnes, B., Lam, A., Lacasse, S., Nadim, F., Sparrevik, M., Vangelsten, B.V., Stumpf, A., Van Den Eeckhaut, M., Hervàs, J., Leroi, E., Intrieri, E., Tofani, V., Agliardi, F., Gili, J., Moya, J., Michoud, C., Derron, M-H., Jaboyedoff, M., Blikra, L-H. (2012) Guidelines for landslide monitoring and early warning systems in Europe – Design and required technology. Deliverable D4.8, EU project SAFELAND, 153 pp. (available at www.Safeland-fp7.eu).

Bernardie S., Desramaut N., Malet J.-P., Gourlay M., Grandjean G. (2015). Prediction of changes in landslide rates induced by rainfall. Landslides (2015) 12:481–494.

Bhandari, R.K. 1988. Special lecture: some practical lessons in the investigation and field monitoring of landslides. In Proceedings of the 5th International Symposium on Landslides, Lausanne. Edited by Ch. Bonnard. A.A. Balkema, Rotterdam, Vol. 2, pp. 1435–1457.

Blikra, L. H., Christiansen, H. H., Kristensen, L., Lovisolo, M. (2015). Characterization, Geometry, Temporal Evolution and Controlling Mechanisms of the Jettan Rock-Slide, Northern Norway. In Engineering Geology for Society and Territory, 2, 273-278. Springer International Publishing.

Broadbent, C.D, Zavodni, Z.M. (1982). Influence of rock structure on stability. Stability in Surface Mining, 3, Soc. of Mining Engineers.

Broccolato M., Cancelli P., Crosta G.B., Tamburini A., Alberto W. (2011) Tecniche di rilievo e monitoraggio della frana di Mont de la Saxe (Courmayeur - AO). XXIV Convegno Nazionale di Geotecnica, "Innovazione Tecnologica nell'ingegneria Geotecnica", Napoli 22-24 june 2011 (in Italian).

Casagli N, Catani F, Del Ventisette C, Luzi G. (2010). Monitoring, prediction, and early warning using ground-based radar interferometry. Landslides. 7: 291–301.

Cappa F., Guglielmi Y., Soukatchoff V.M., Mudry J., Bertrand C., Charmoille A. (2004). Hydromechanical modeling of a large moving rock slope inferred from slope levelling coupled to spring long-term hydrochemi-cal monitoring: example of the La Clapiere landslide (Southern Alps, France). Journal of Hydrology, 291(1), 67-90.

Crosta, G.B. (2013) Revisione dei valori Soglia da dati GB_InSAR a seguito dell'evento novembre 2012. Research Report, Università degli Studi di Milano Bicocca, ARPA-CMG Lombardia, 21 pp (in Italian)

Crosta, G., Agliardi, F., Frattini, P. (1999). Convenzione di studio sulla Frana del Ruinon (Valfurva, Sondrio). Technical report, Regione Lombardia–Dipartimento di Scienze Geologiche e Geotecnologie, Università di Milano-Bicocca, 197 pp (in Italian).

Crosta G., Zanchi A. (2000) Deep seated slope deformations: huge, extraordinary, enigmatic phenomena. Proceed. VIII Int. Symp. on Landslides, ISL, Cardiff 2000, 1, 351-358.

Crosta, G.B., Agliardi, F. (2003). Failure forecast for large rock slides by surface displacement measurements. Canadian Geotechnical Journal. 40, 1: 176-191.

Crosta, G.B., Castellanza R., Frattini, P., Broccolato M., Bertolo, D., Cancelli P., Tamburini A, (2012) Comprehensive understanding of a rapid moving rockslide: the Mt de la Saxe landslide. MIR 2012 XIV Ciclo di Conferenze di Meccanica e Ingegneria delle Rocce - Nuovi metodi di indagine, monitoraggio e modellazione degli ammassi rocciosi, 231-250 (in Italian).

Crosta, G.B., di Prisco, C., Frattini, P., Frigerio, G., Castellanza, R., Agliardi, F. (2014). Chasing a complete understanding of the triggering mechanisms of a large rapidly evolving rockslide. Landslides, 11, 5, 747-764, doi: 10.1007/s10346-013-0433-1.

Crosta, G.B., Frattini, P., Agliardi, F., Sosio, E., Rocchi, G., Vaciago, G., Callerio, A., Fontana, M., Previtali, F., Spickermann, A., Malet, JP., Picarelli, L., Santo, A., Di Crescenzo, G., Springman, S.,. Alonso, E., Pineda, J., Pinyol, N.M., Romero, E., Pitilakis, K., Fotopoulou, S., Kakderi, K., Riga, E., Ktenidou, O., (2010) . Landslide triggering mechanisms in Europe – Overview and State of the Art, Deliverable D1.1, EU project SAFELAND, 373 pp. (available at www.Safeland-fp7.eu)

Cruden, D. M., Masoumzadeh, S. (1987). Accelerating creep of the slopes of a coal mine. Rock Mechanics and Rock Engineering, 20(2), 123-135.

Del Ventisette, C., Casagli, N., Fortuny-Guasch, J., Tarchi, D. (2012) Ruinon landslide (Valfurva, Italy) activity in relation to rainfall by means of GBInSAR monitoring. Landslides 9:497–509, DOI 10.1007/s10346-011-0307-3

Ferretti, A., Prati, C., Rocca, F., (2001). Permanent scatterers in SAR interferometry. Geoscience and Remote Sensing, IEEE Transactions on, 39(1), 8-20.

Ferretti, A., Fumagalli, A., Novali, F., Prati, C., Rocca, F., Rucci, A., (2011). A new algorithm for processing interferometric data-stacks: SqueeSAR™. IEEE Trans. Geosci. Remote Sens. 49 (9), 3460–3470.

Fukuzono, T. (1985). A new method for predicting the failure time of a slope. In: Proc. 4th Inter. Conference and Field Workshop on Landslides, Tokyo, Tokyo University Press: 145–150.

Guglielmi Y., Cappa F., Binet S. (2005). Coupling be-tween hydrogeology and deformation of mountainous rock slopes: Insights from La Clapière area (southern Alps, France). Comptes Rendus Geoscience, 337(13), 1154-1163.

Helmstetter, A., S. Garambois (2010) Seismic monitoring of Séchilienne rockslide (French Alps): Analysis of seismic signals and their correlation with rainfalls, J. Geophys. Res., 115, F03016, doi:10.1029/2009JF001532.

Herrera G., Fernández-Merodo J.A., Mulas J., Pastor M., Luzi G., Monserrat O. (2009). A landslide forecasting model using ground based SAR data: The Portalet case study. Engineering Geology, 105(3), 220-230.

Intrieri, E., Gigli, G., Mugnai, F., Fanti, R., Casagli, N. (2012). Design and implementation of a landslide early warning system. Engineering Geology, 147, 124-136.

Michoud, C., Bazin, S., Blikra, L. H., Derron, M. H., Jaboyedoff, M. (2013). Experiences from site-specific landslide early warning systems. Natural Hazards and Earth System Science, 13(10), 2659-2673.

Mufundirwa, A., Fujii, Y., Kodama, J. (2010) A new practical method for prediction of geomechanical failure-time. Int. J. Rock Mech. Min. Sci., 47, 1079-1090

Oppikofer, T., Jaboyedoff, M., Pedrazzini, A., Derron, M.-H., Blikra, L. H. (2011), Detailed DEM analysis of a rockslide scar to characterize the basal sliding surface of active rockslides, J. Geophys. Res., 116, F02016, doi:10.1029/2010JF001807.

Rose, N. D., Hungr, O. (2007). Forecasting potential rock slope failure in open pit mines using the inverse-velocity method. International Journal of Rock Mechanics and Mining Sciences, 44(2), 308-320.

Saito, M., Uezawa, H. (1961). Failure of soil due to creep. In: Proceedings of the 5th International Conference on Soil Mechanics and Foundation Engineering. 1: 315–318.

Sornette, D., Helmstetter, A., Andersen, J. V., Gluzman, S., Grasso J.R. and Pisarenko, V. (2004) Towards landslide prediction: two case studies, Physica A, 338, 605-632.

Strozzi, T., Delaloye, R., Kääb, A., Ambrosi, C., Perruchoud, E., Wegmüller, U. (2010), Combined observations of rock mass movements using satellite SAR interferometry, differential GPS, airborne digital photogrammetry, and airborne photography interpretation, J. Geophys. Res., 115, F01014, doi:10.1029/2009JF001311.

Tarchi, D., Casagli, N., Moretti, S., Leva, D., Sieber, A. J. (2003), Monitoring landslide displacements by using ground-based synthetic aperture radar interferometry: Application to the Ruinon landslide in the Italian Alps, J. Geophys. Res., 108, 2387, doi:10.1029/2002JB002204, B8.

Vallet A., Charlier J.B., Fabbri O., Bertrand C., Carry N., Mudry J. (2015). Functioning and precipitation-displacement modelling of rainfall-induced deep-seated landslides subject to creep deformation. Landslides, 1-18.

Voight, B. (1988). A method for prediction of volcanic eruption. Nature. 332: 125–130.

Zangerl C., Eberhardt E., Perzlmaier S. (2010). Kinematic behaviour and velocity characteristics of a complex deep-seated crystalline rockslide system in relation to its inter-action with a dam reservoir. Engineering Geology, 112(1), 53-67.

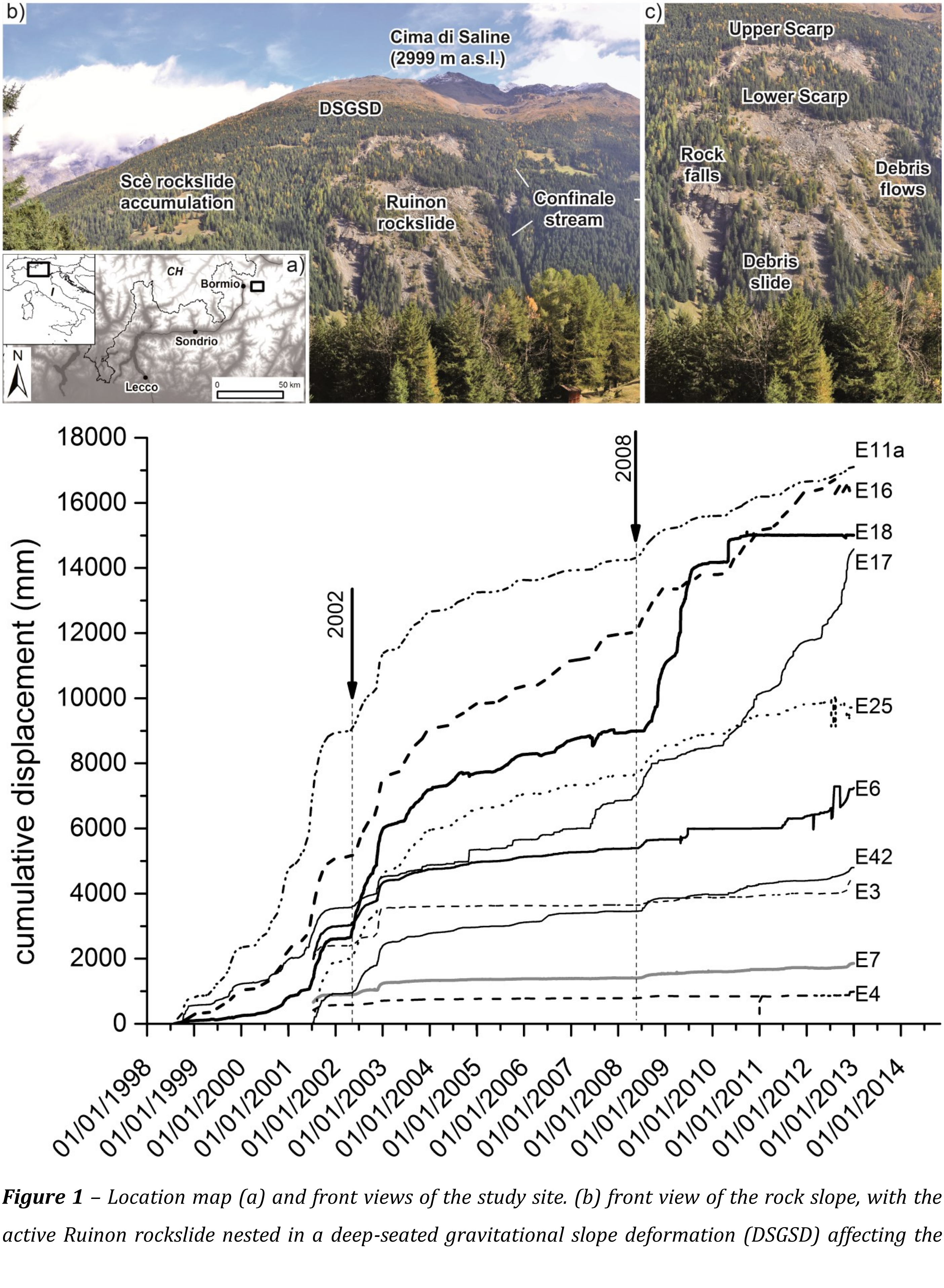

Figure 1 *– Location map (a) and front views of the study site. (b) front view of the rock slope, with the active Ruinon rockslide nested in a deep-seated gravitational slope deformation (DSGSD) affecting the*

slope up to the Cima di Saline ridge; (c) front view of the slope sector affected by the Ruinon rockslide (photo: October 2014).

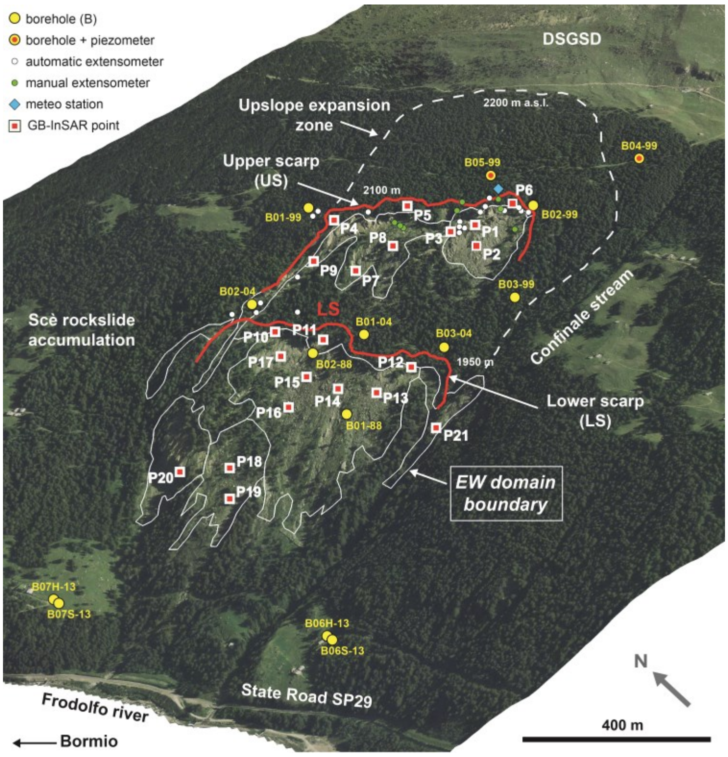

Figure 2 *– 3D view of the Ruinon rockslide showing: the main morphological features and areas of possible rockslide upslope expansion (white dashed line); the location of boreholes in Fig. 3; the layout of the ground-based monitoring network implemented since 1997 (see legend); the location of 21 GB-InSAR streaming points (virtual monitoring network) used for early warning in the outlined "Early Warning domains" (see text and Fig. 8).*

Figure 3 – *Geological cross section of the Ruinon rockslide (updated after Crosta and Agliardi, 2003) showing the main rockslide features, interpreted shear surfaces, site investigations, and general distribution of the surface displacements recorded by the GB-InSAR system in the 2006-2014 period. The location and look angle of the GB-InSAR system is showed in the inset.*

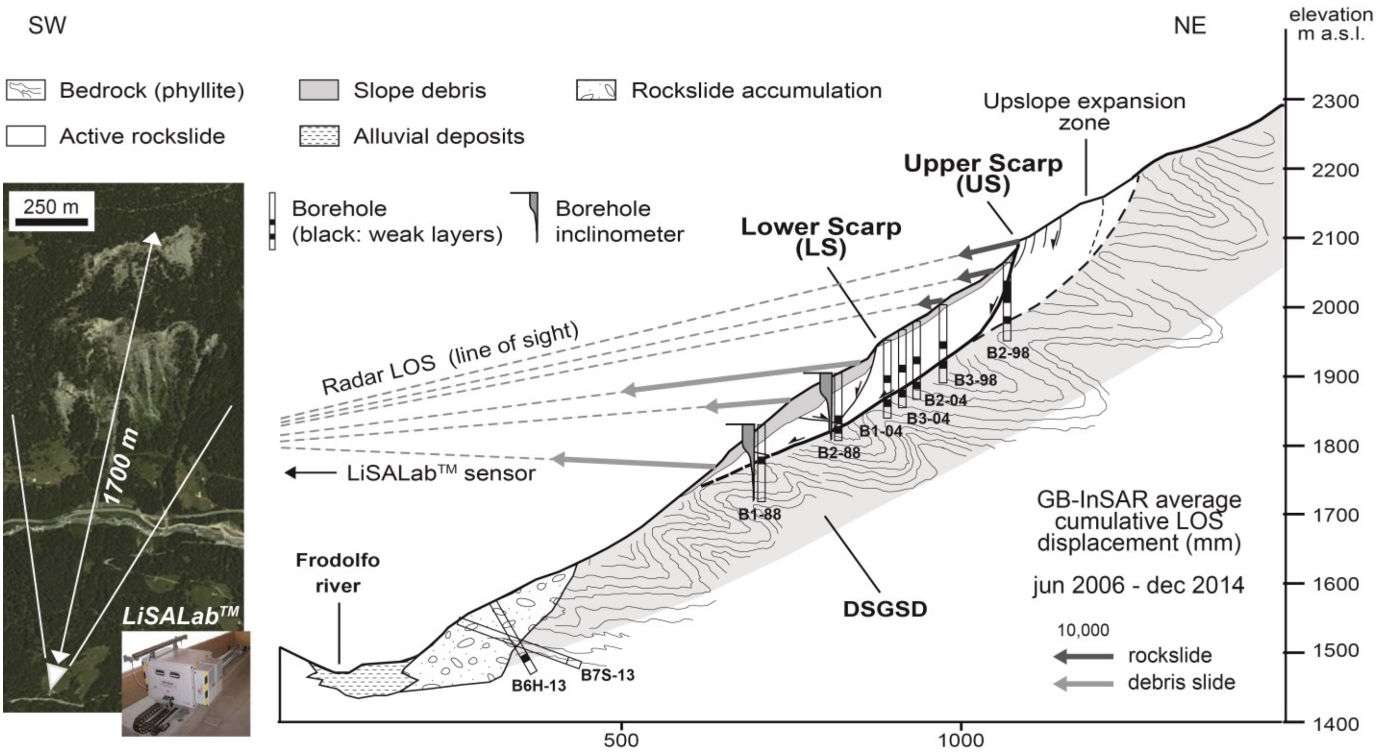

Figure 4 - *Long term evolution of the Ruinon rockslide (1998-2014) from ground-based displacement measurements by wire extensometers. See figure 2 for position of extensometers.*

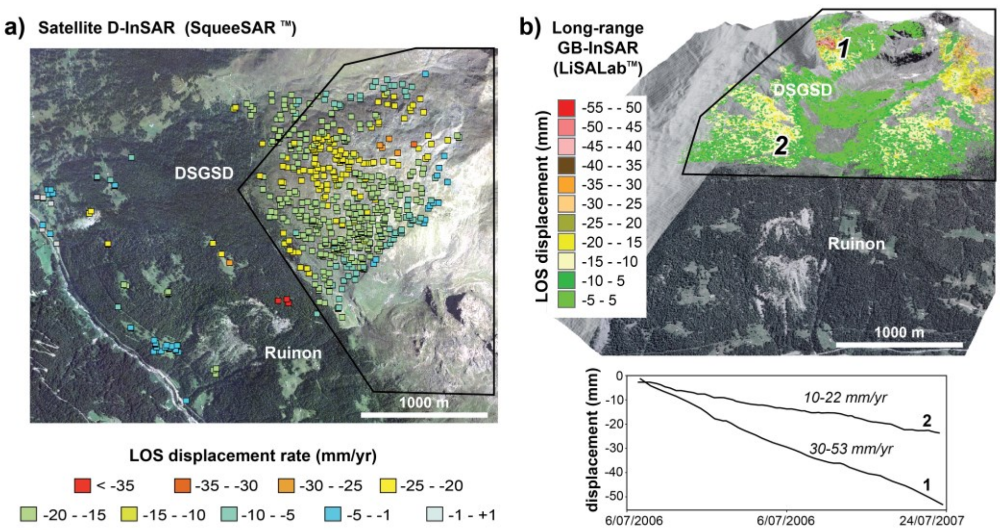

Figure 5 *– Spatially-distributed deformation monitoring of the deep-seated gravitational slope deformation (DSGSD) affecting the entire Cima di Saline slope (see Fig. 1). a) displacement rates obtained by SqueeSAR™ satellite radar interferometry (descending Radarsat S3, 2003-2008; courtesy*

Telerilevamento Europa srl); b) 3D map and plots of cumulative displacements measured during a 1-year long-range GB-InSAR monitoring experiment (2006-2007; courtesy LiSALab srl). Negative values: LOS displacements towards the sensor.

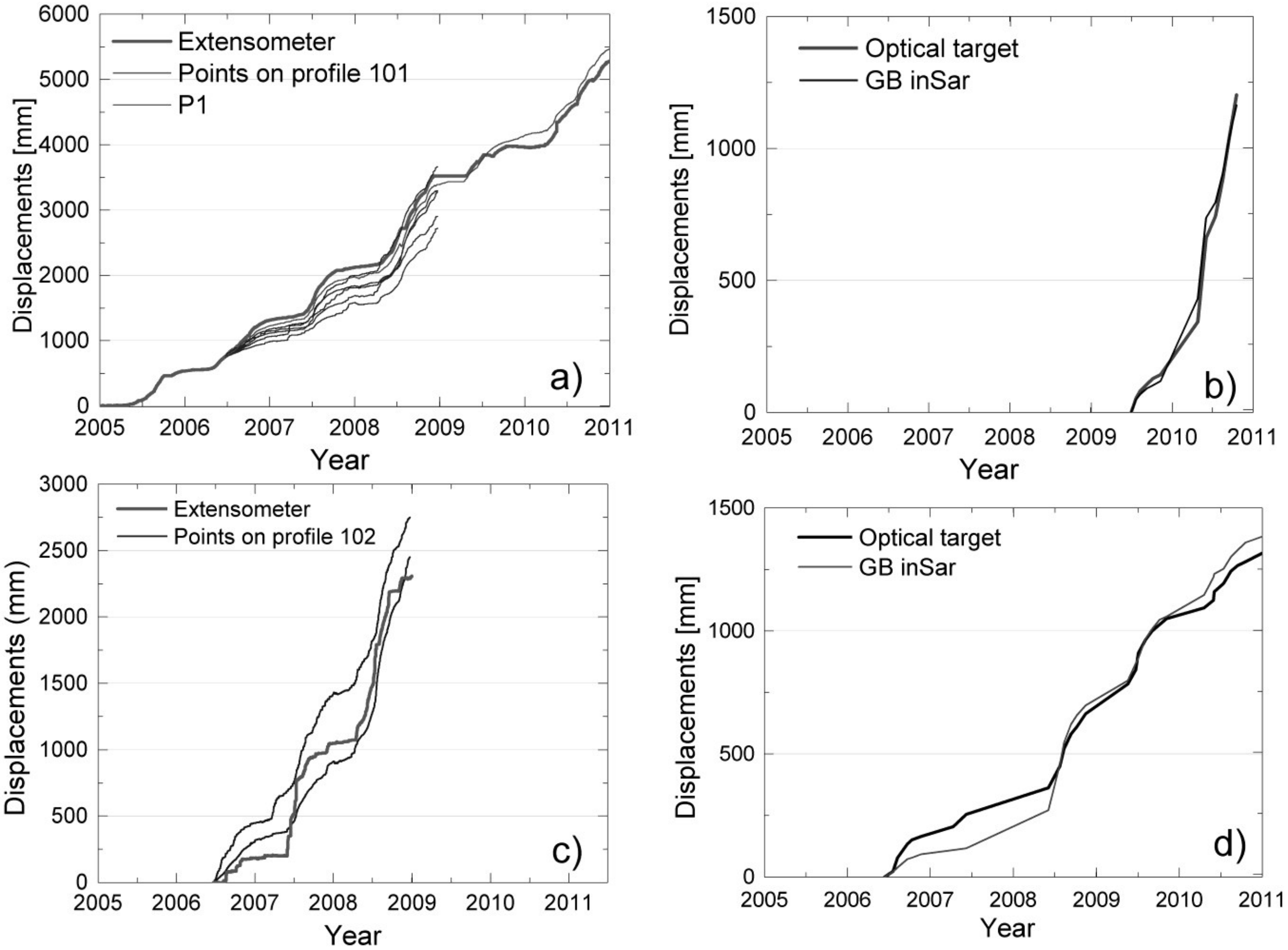

Figure 6 *- Comparison among time series of cumulative displacement for GB-InSAR and in situ instrumentation. The data (positive values: LOS displacements towards the sensor) refer to GB-InSAR points located in the immediate vicinity of in situ monitoring devices (extensometers and optical targets). See Figure 2 for the location of the profiles and monitoring points.*

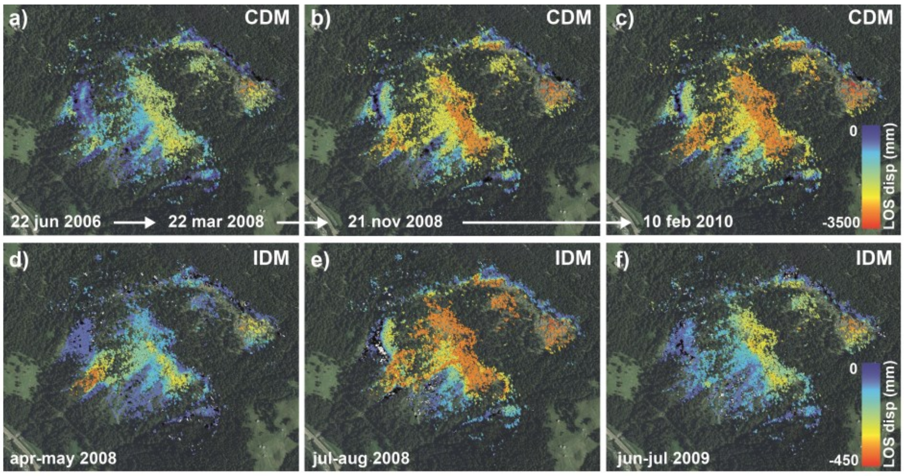

Figure 7 *– Examples of multi-temporal analysis of GB-InSAR: a, b, c) Cumulative Displacement Maps (CDM); d, e, f) Incremental Displacement Maps (IDM). Portions of different degree and style of activity are recognized. (Positive values: LOS displacements towards the sensor).*

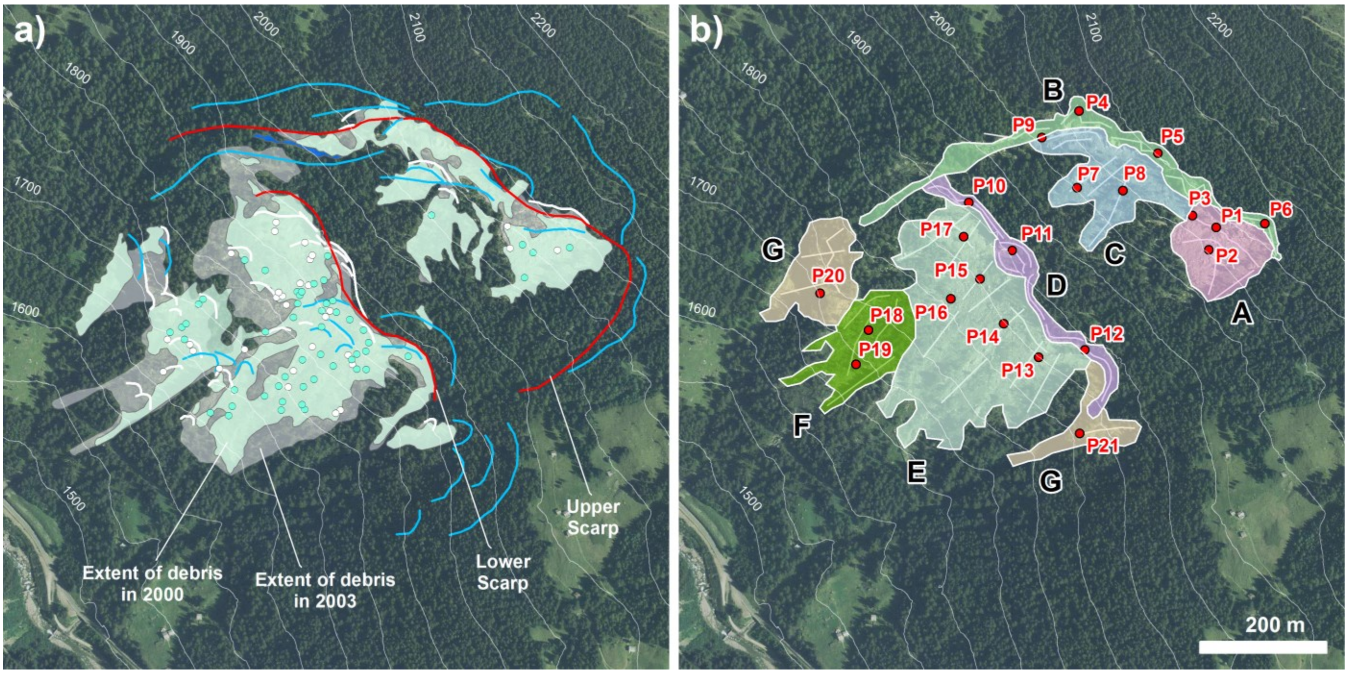

Figure 8 *- Major elaboration steps followed for the rockslide zonation into homogeneous "Early Warning domains". a) geomorphological mapping attained from 9 aerial photo leverages. Legend: lines are main scarps and fractures; dots are large blocks; polygons in different colours map the extent of scree slope deposits. b) identification of homogeneous sub-areas (13), indicated by colours and identified with respect to: involved materials (rock mass or debris), style of activity, displacement trends, and inferred instability mechanisms. Sub-areas with similar behaviours were merged into 7 "Early Warning domains" (A to G). Light coloured lines and dots represent the selected virtual sensors for the extraction of time histories. See text for explanation.*

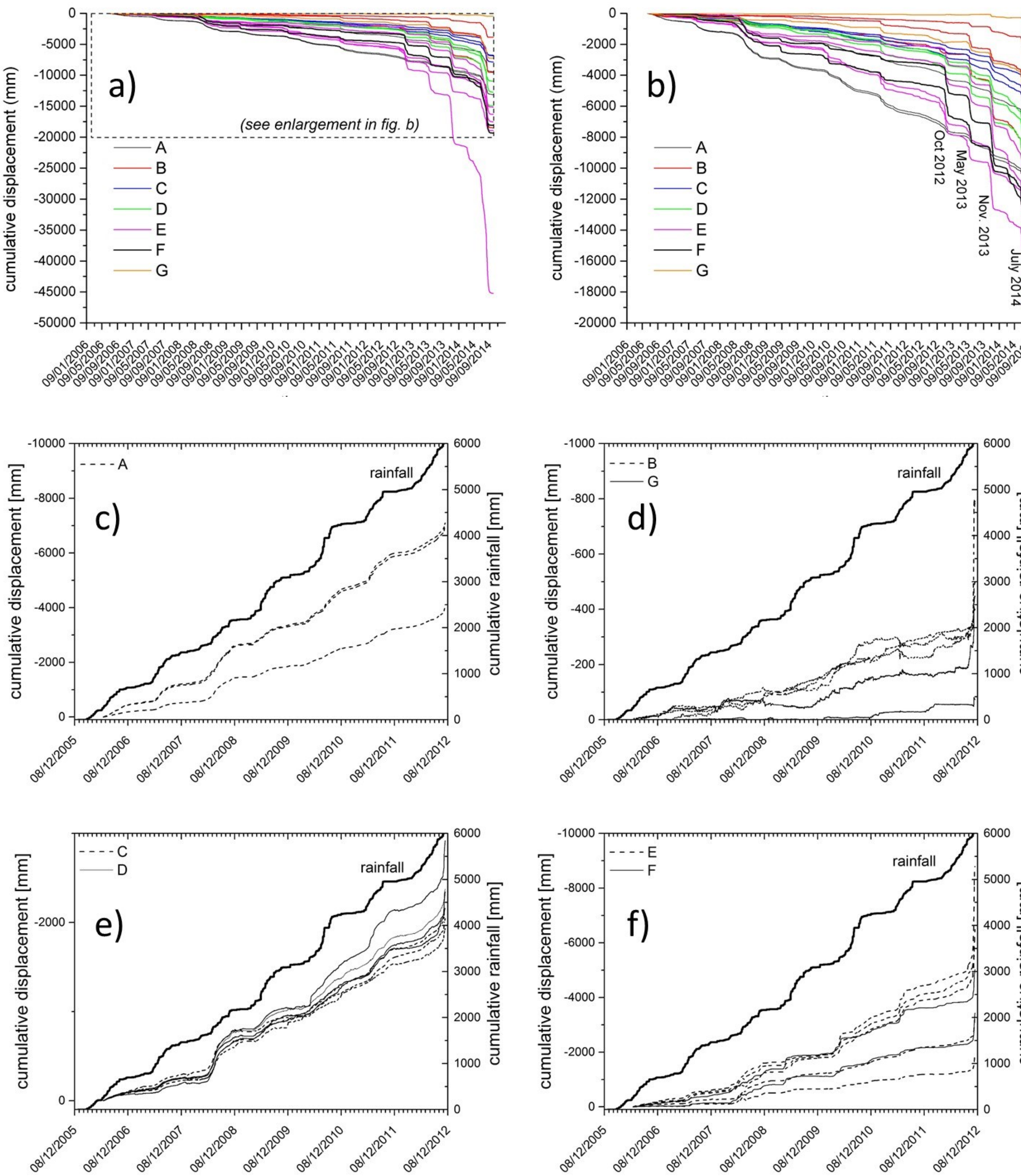

Figure 9 *- Cumulative displacement versus cumulative rainfall (upper curve, same in all the plots) over the 2006-2012 monitoring period for various monitored streaming points in different Early Warning domains (Fig. 8; debris slope: A, C and D, E and F; rock slope: B and G) and grouped according to the different response to triggering events.*

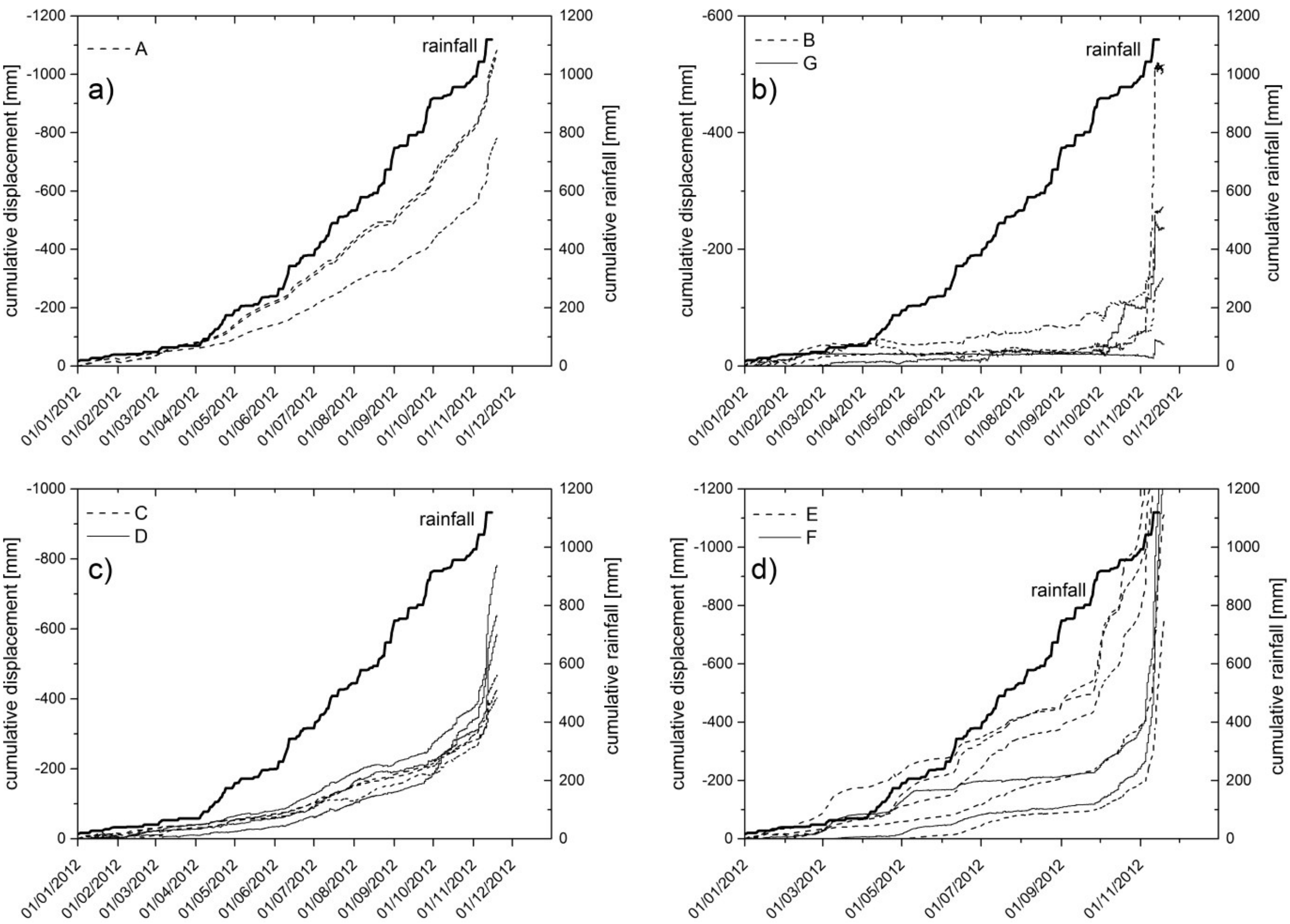

Figure 10 - *Cumulative displacement versus cumulative rainfall for the year 2012, for various monitored streaming points in different Early Warning domains (Fig. 8; debris slope: A, C and D, E and F; rock slope: B and G) and grouped according to the different response to triggering events. October – November 2012 event was characterized by rain and contemporaneous snowmelt of an early snowfall. Positive values: LOS displacements towards the sensor.*

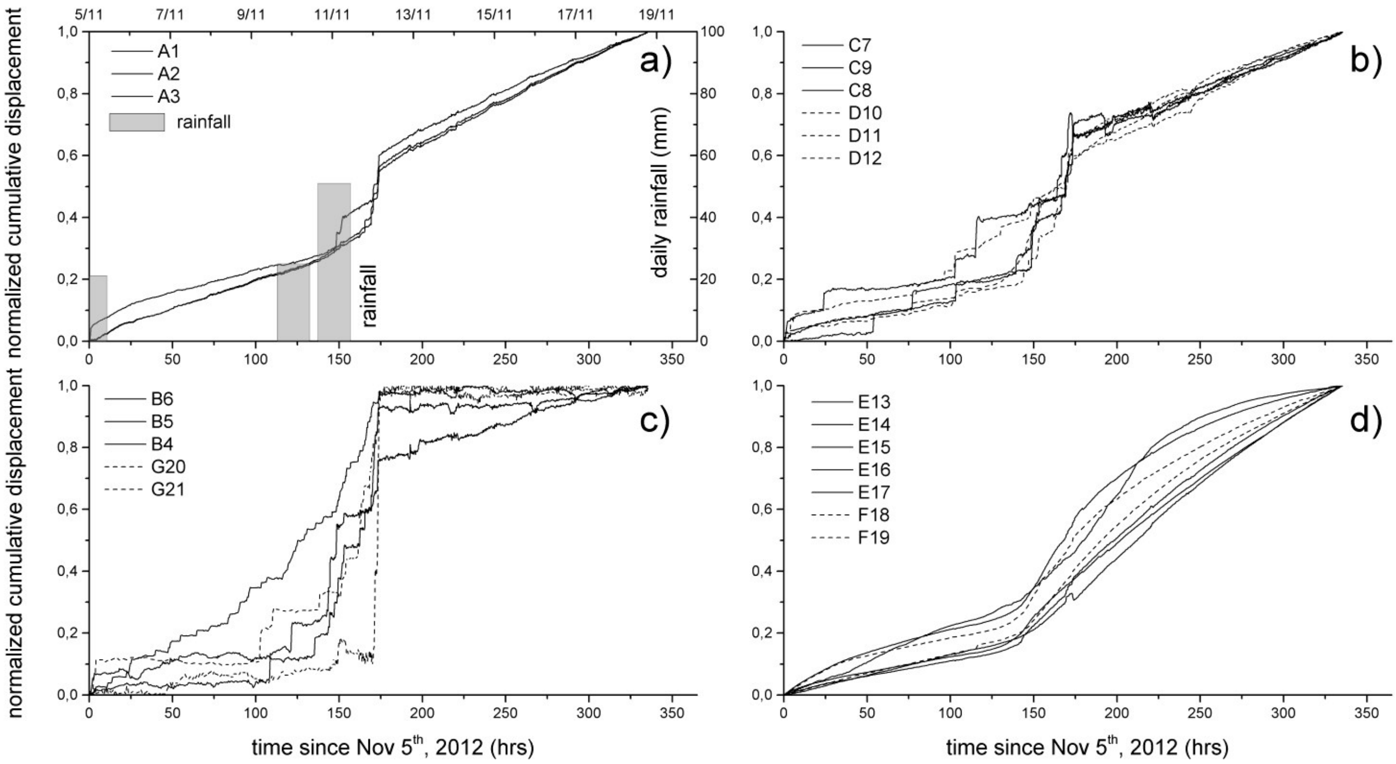

Figure 11 *– Plots of normalized cumulative displacements for the November 2012 acceleration period subdivided according to the domain (A to G) with respect to rainfall distribution (bar chart). See Figure 2 and 8 for position of streaming points.*

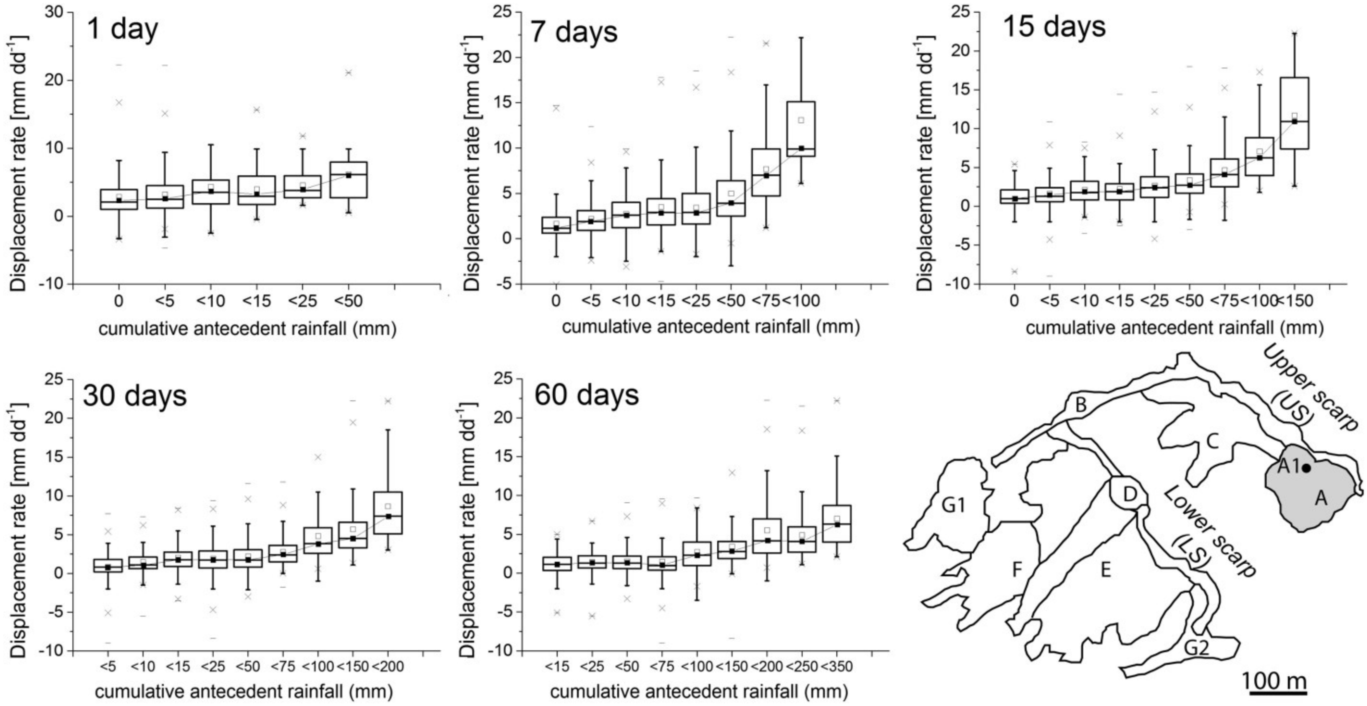

***Figure 12** – Box plots of displacement rates (mm/hr) for a streaming point (A1 see inset in the lower right hand corner, chosen as example, and extracted by the GB-InSAR data series for different intervals of antecedent rainfall (1, 7, 15, 30, 60 days). Box plots include data within 25 and 75 percentiles; the mean values, 99° percentiles and extreme values are shown.*

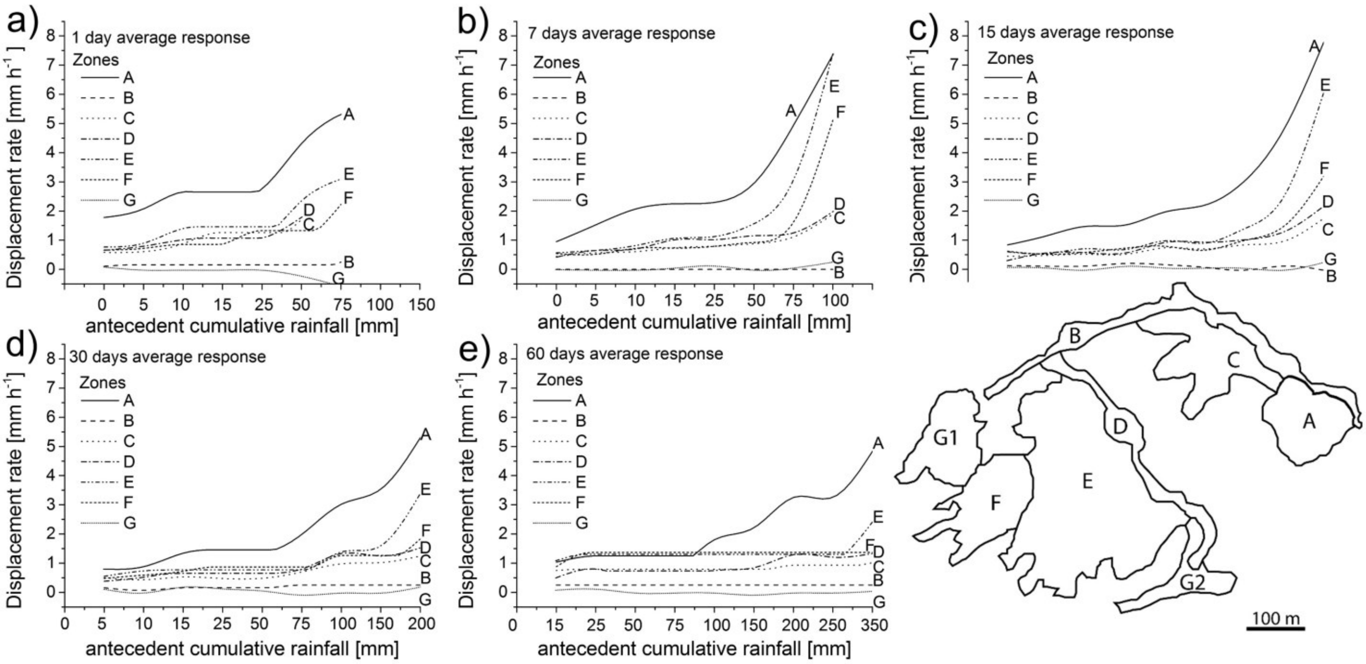

Figure 13 *– Relationship between displacement rates and antecedent rainfall cumulated over a) 1, b) 7, c) 15, d) 30, e) 60 days. Data are collected in the period June 2006-June 2011 and refer to different Early Warning domains and different periods over which rainfall are cumulated*

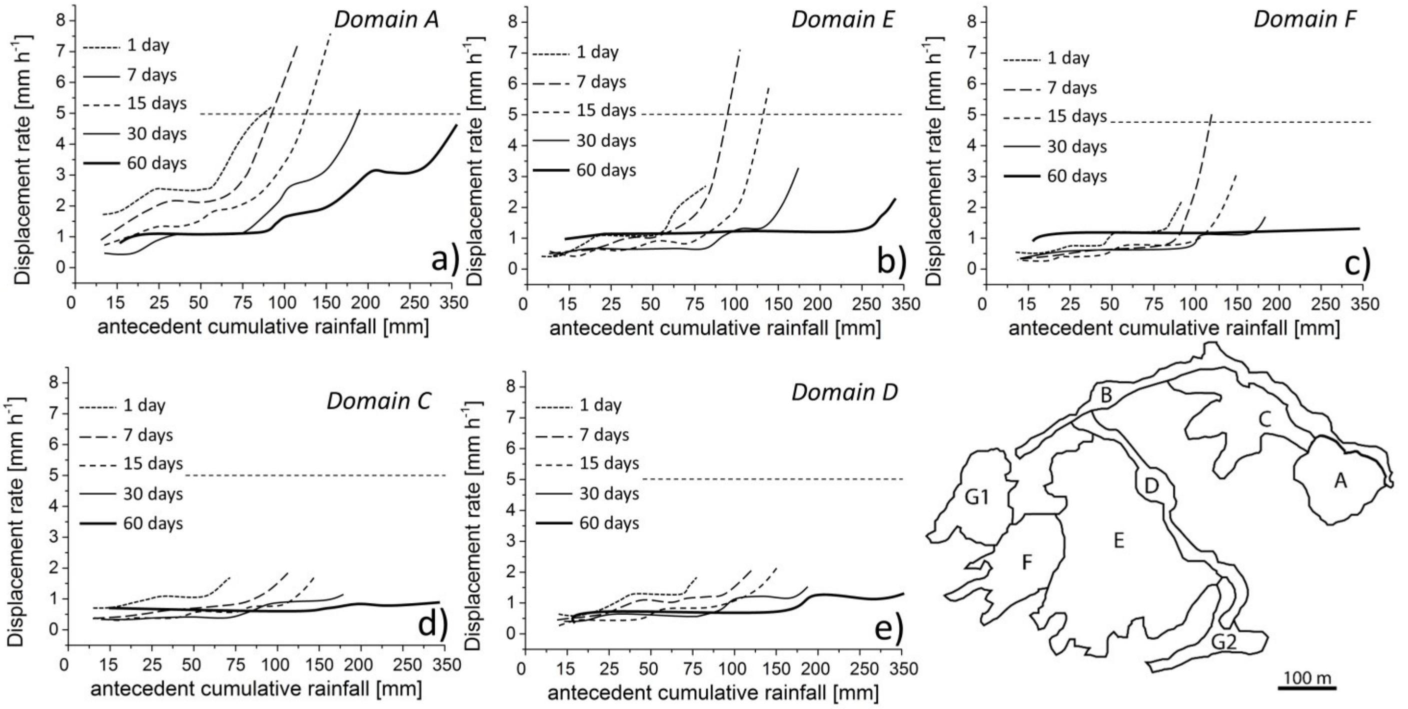

Figure 14 *– Relationship between displacement rates and antecedent rainfall cumulated over a) 1, b) 7, c) 15, d) 30, e) 60 days. Data are collected in the period June 2006-June 2011 and refer to different Early Warning domains.*

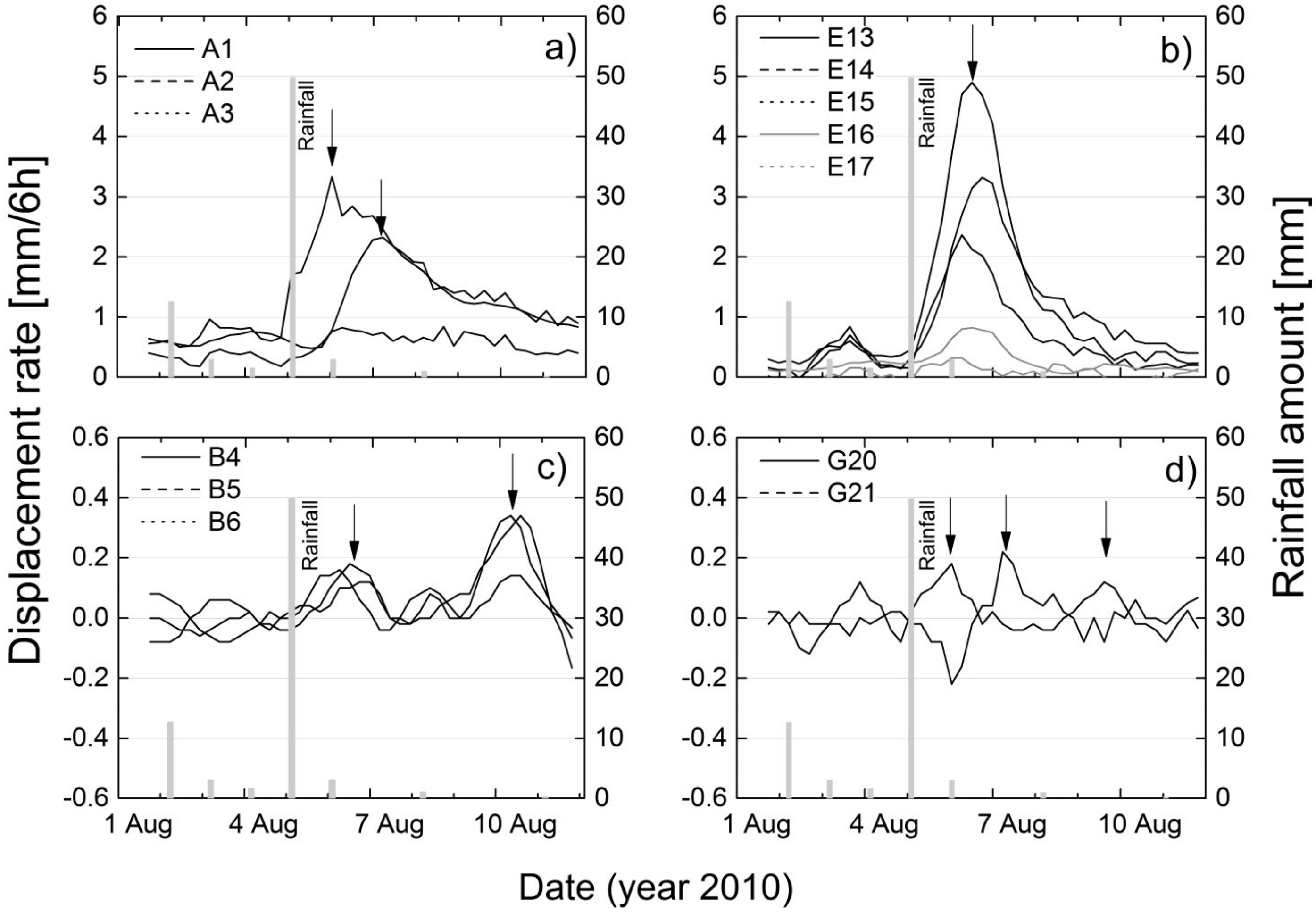

Figure 15 *– Different types of rainfall-displacement rate response to the same rainfall event (bar charts) for different rockslide sectors, outlining the potential of Early Warning based on rainfall thresholds in different EW domains. Displacement rates are averaged on 5 points measurements. Note that the displacement scales are different. Arrows point to the peaks in displacement rate and the different positioning in time for different domains or points within the same domain. See Fig. 2 for position of each streaming point.*

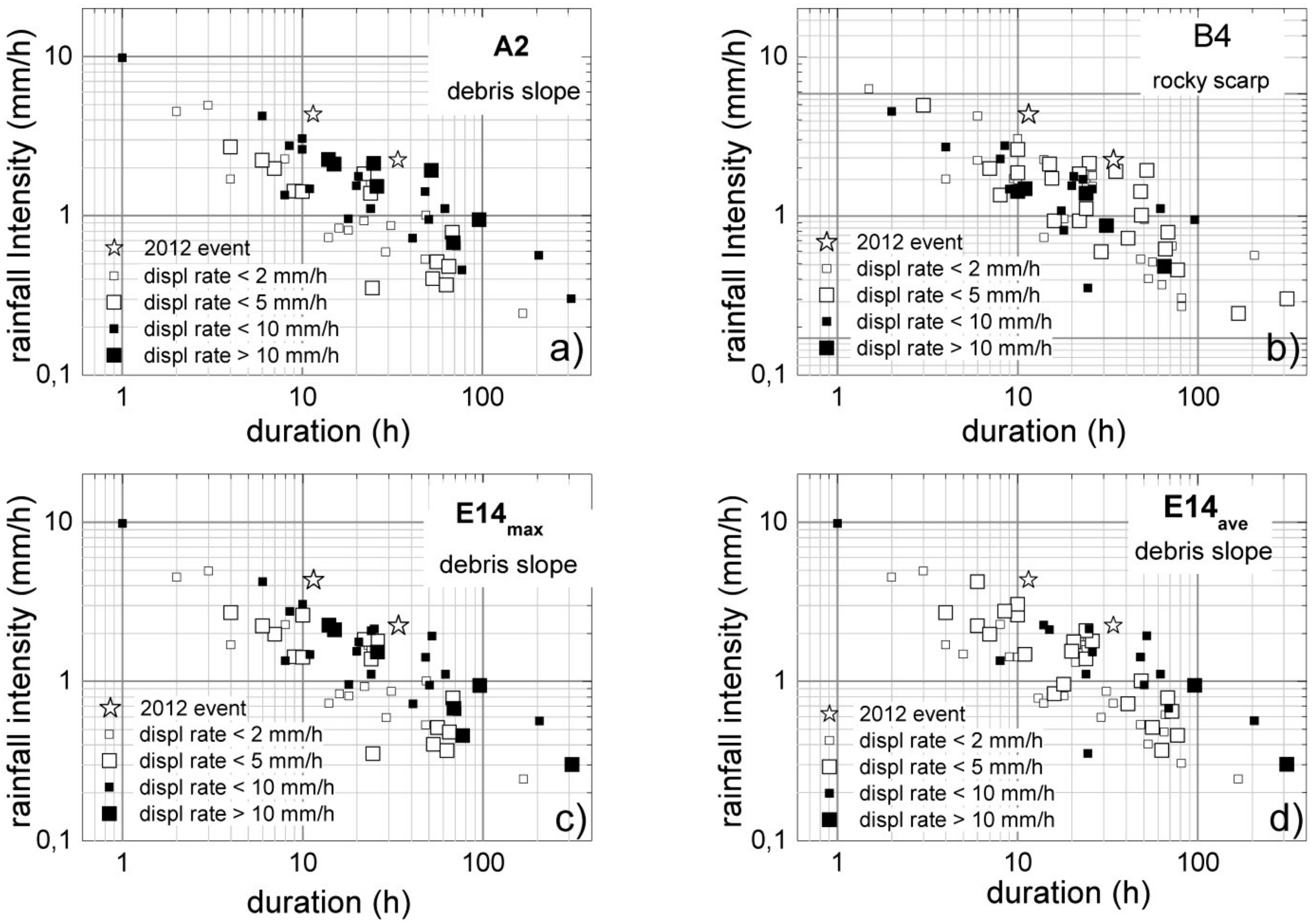

Figure 16 *– Intensity-duration plots for a total of 70 rainfall events recorded from May 2006 to November 2012. Couples of ID values are classified according to the displacement rates observed at different rockslide sectors: a) debris slope in Domain A (streaming point A2), b) rocky scarp Domain B (US; streaming point B4); c) and d) debris slope E14 Domain E, maximum and mean displacement rates, respectively. See Fig. 2 for position of each streaming point.*

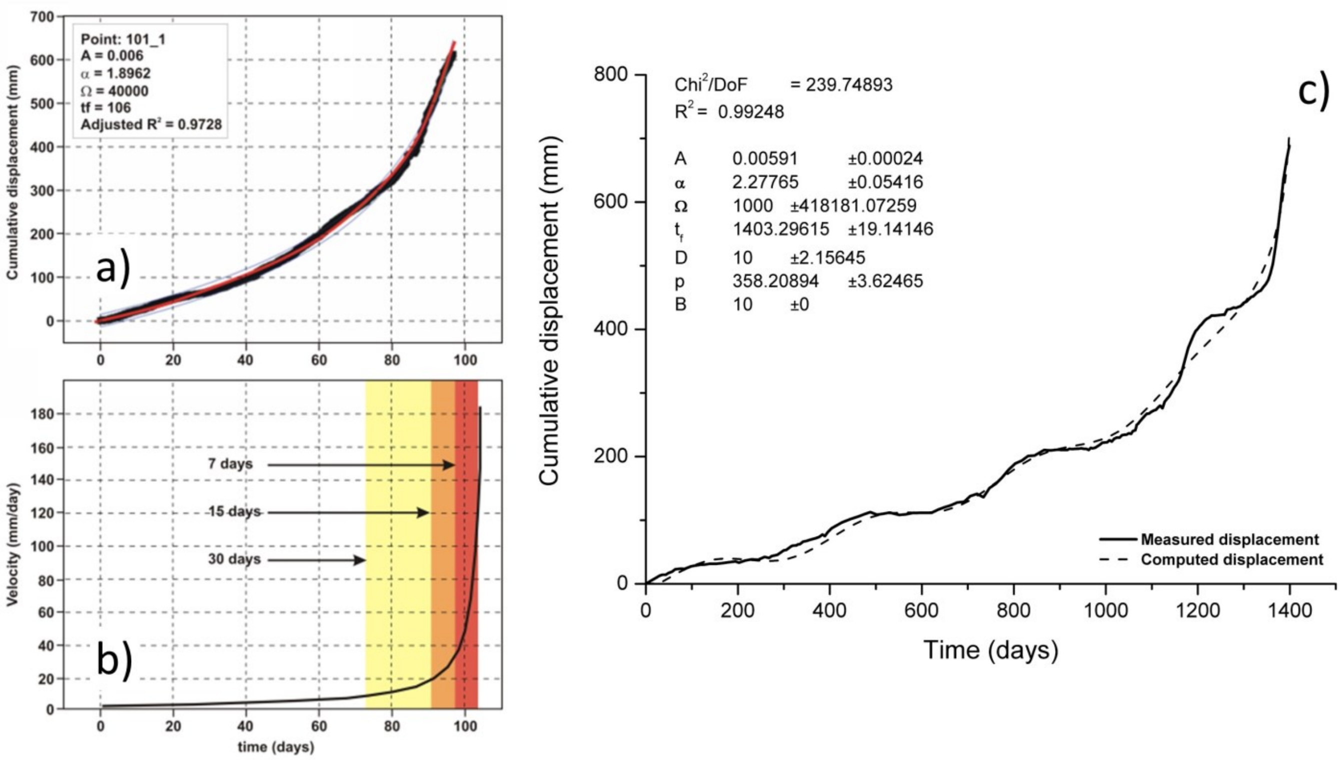

Figure 17 *– a) fitting of the displacement data for an accelerating episode by the approach proposed by Crosta and Agliardi (2003); b) conversion of the best fit relationship in terms of velocity and identification of the velocity thresholds at different time intervals (7, 15 and 30 days) before expected collapse; c) effect of a periodic component added to the approach proposed by Crosta and Agliardi (2003) to simulate the effect of seasonal reactivation till collapse time.*

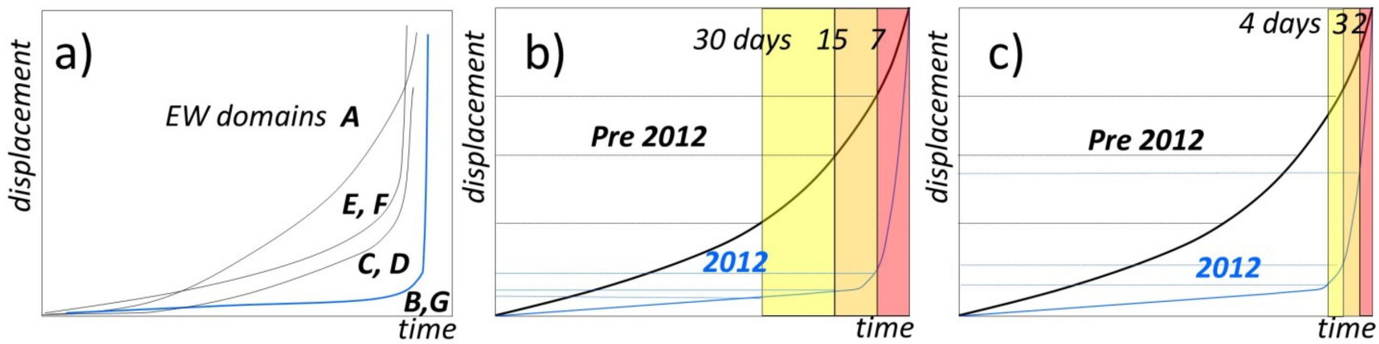

Figure 18 *– Adaptive approach for the definition of alert velocity thresholds depending on the evolution of rockslide behaviour (e.g. transition rock mass – disrupted rock mass – granular "soil") and the hydrological trigger intensity (e.g. intense/prolonged rainfall and snowmelt). a) initial characteristic displacement versus time relationships defined for each EW domain; b) observed changes in the event displacement curves for the same area during two events (pre 2012 and 2012).The 7, 15 and 30 day lines before expected collapse are drawn and the unsuitability of these time intervals for EW procedures is evident by the change in the 2012 curve; c) definition of new threshold values and time intervals (4, 3 and 2 days) to adapt to the new behaviour of the rockslide mass. Curves are the same as in b).*

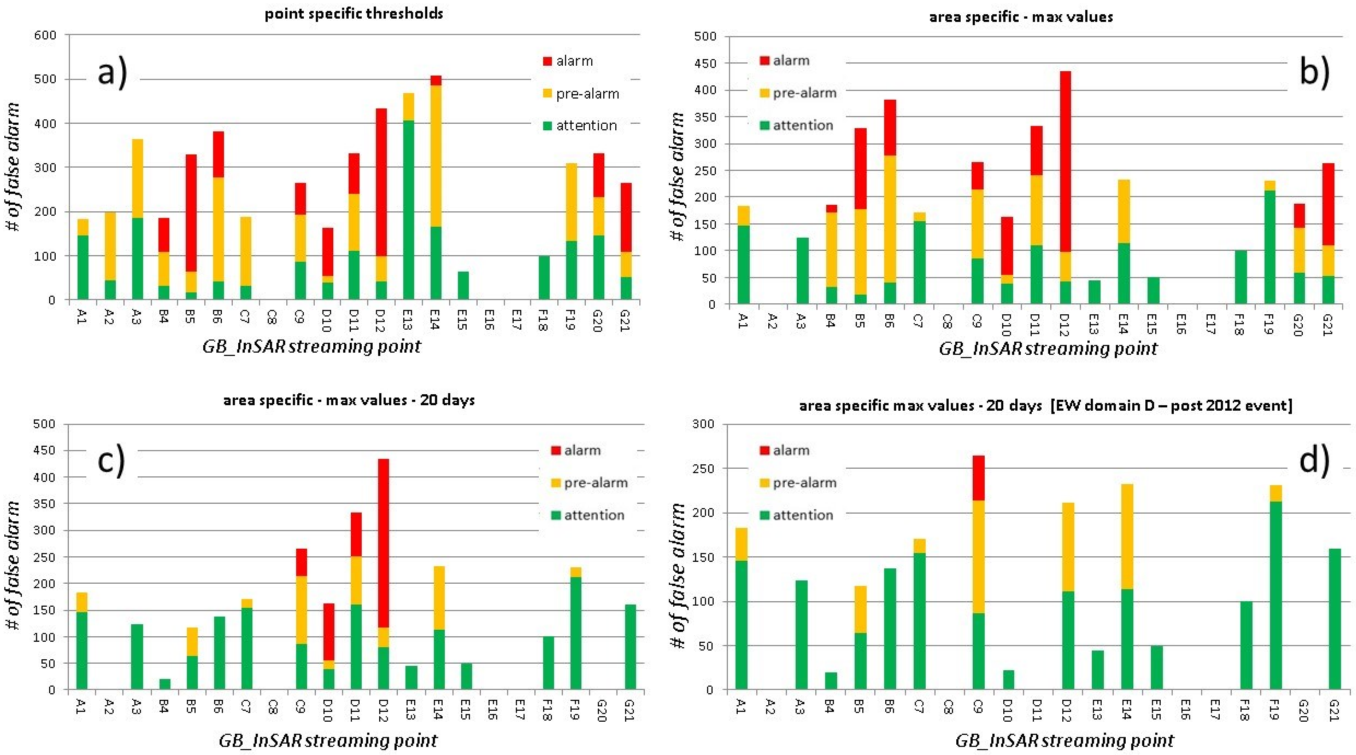

Figure 19 *– Testing different threshold values for the minimization of false alarms, obtained by successively applying different thresholds to the entire set of records (1997 to 2014). a) Exceedance of the threshold value for a single streaming point in a specific EW domain; b) exceedance of the maximum threshold value within each EW domain; c) adoption of threshold values computed over a longer time interval (20 days); d) updating of the thresholds for EW domain D after the 2012 event for which a strong change in behaviour of domain D was observed. See Fig. 2 for position of each streaming point.*